Auditory Cortical Onset Responses Revisited. I. First-Spike Timing

PETER HEIL
Department of Psychology, Monash University, Clayton, Victoria 3168, Australia

Heil, Peter. Auditory cortical onset responses revisited. I. First-spike timing. *J. Neurophysiol.* 77: 2616–2641, 1997. Sound onsets are salient and behaviorally relevant, and most auditory neurons discharge spikes locked to such transients. The acoustic parameters of sound onsets that shape such onset responses are unknown. In this paper is analyzed the timing of spikes of single neurons in the primary auditory cortex of barbiturate-anesthetized cats to the onsets of tone bursts. By parametric variation of sound pressure level, rise time, and rise function (linear or cosine-squared), the time courses of peak pressure, rate of change of peak pressure, and acceleration of peak pressure during the tones' onsets were systematically varied. For cosine-squared rise function tones of a given frequency and laterality, any neuron's mean first-spike latency was an invariant and inverse function of the maximum acceleration of peak pressure occurring at tone onset. For linear rise function tones, latency was an invariant and inverse function of the rate of change of peak pressure. Thus latency is independent of rise time or sound pressure level per se. Latency-acceleration functions, obtained with cosine-squared rise function tones under different stimulus conditions (frequency, laterality) from any given neuron and across the neuronal pool, were of strikingly similar shape. The same was true for latency–rate of change of peak pressure functions obtained with linear rise function tones. Latency–acceleration/rate of change of peak pressure functions could differ in their extent and in their position within the coordinate system. The positional differences reflect neuronal differences in minimum latency L_{min} and in a sensitivity S to acceleration and rate of change of peak pressure (transient sensitivity), a hitherto unrecognized neuronal property that is distinctly different from firing threshold. Estimates of L_{min} and S, which were derived by fitting a simple function to the neuronal latency–acceleration/rate of change of peak pressure functions, were independent of rise function. On average, L_{min} decreased with increasing characteristic frequency (CF), but varied widely for neurons with the same CF. S varied with CF in a fashion similar to the cat's audiogram and, for a given neuron, varied with frequency. SD of first-spike latency was roughly proportional to the slope of the functions relating latency to acceleration/rate of change of peak pressure. Thus SD increased exponentially, rather than linearly, with mean latency, and did so at about twice the rate for linear than for cosine-squared rise function tones. The proportionality coefficients were quite similar across the neuronal pool and similar for both rise functions. Minimum SD increased nonlinearly with increasing L_{min}. These findings suggest a peripheral origin of S and a peripheral establishment of latency–acceleration/rate of change of peak pressure functions. Because of the striking similarity in the shapes of such functions across the neuronal pool, sound onsets will produce orderly and predictable spatiotemporal patterns of first-spike timing, which could be used to instantaneously track rapid transients and to represent transient features by partly scale-invariant temporal codes.

INTRODUCTION

Natural acoustic signals, including many of those used by animals and humans for auditory communication, are spectrally and temporally complex. A recent study has emphasized the importance of the temporal structure of the envelope by showing that it can convey an unexpected amount of information needed for speech recognition (Shannon et al. 1995). Animal studies have shown that throughout the auditory pathway neurons can be excited by rapid temporal changes in stimulus envelopes, provided that the stimuli have an adequate spectral content. In many studies researchers have used stimuli with repetitive envelope fluctuations, such as periodically amplitude-modulated sinusoids or noise or click trains, and have demonstrated that neuronal responses can be locked to the individual repetitive envelope fluctuations (e.g., auditory nerve: Joris and Yin 1992; cochlear nucleus: Frisina et al. 1985; Rhode and Greenberg 1994; inferior colliculus: Heil et al. 1995; Langner and Schreiner 1988; Rees and Møller 1983; thalamus: Rouiller et al. 1981; cortex: Eggermont 1993; Schreiner and Urbas 1988).

A particularly salient temporal envelope change is the onset of a sound, and nearly all neurons along the auditory pathway respond briskly to such a transient. For example, all physiologically classified neuron types of the cochlear nucleus, with the exception of buildup neurons in the dorsal division, display an initial peak in their poststimulus time histograms recorded in response to short tone bursts (e.g., Rhode and Greenberg 1992). This peak reflects the locking of the neuron's initial spike(s) to the tone's onset, and therefore such responses or response components are sometimes referred to as onset responses. Because of the demonstrated phase-locking of spikes to amplitude-modulated signals or click trains, such signals may constitute a rapid series of like onsets for a neuron. In fact, Rhode and Greenberg (1992) have noted that cochlear nucleus neurons, classified as onset units, phase-lock with high precision also to low-frequency signals (sinusoidal carriers and amplitude-modulated sounds) ''. . . responding as if each cycle is an effective excitatory stimulus'' (p. 100). Onset response components are also evident in the discharge patterns of neurons in locations higher up the pathway, such as the medial geniculate or the auditory cortex (for review see Clarey et al. 1992). Onset responses appear to be least vulnerable to the effects of anesthesia (Zurita et al. 1994), and the responses of neurons in the auditory cortices of chloralose- and barbiturate-anesthetized animals are dominated by discharges locked to the stimulus onset (e.g., Brugge et al. 1969; Phillips 1988; Zurita et al. 1994).

Although it is widely accepted that the initial discharges of most auditory neurons are evoked by stimulus onset, little attention has been given to the question of which physical parameters of the stimulus onset actually shape a neuron's onset response. When auditory neurons are probed with nar-

 0022-3077/97 $5.00

rowband stimuli, such as pure tone bursts, the effects of the abruptness of the amplitude change on the short-term frequency spectrum (e.g., Durrant and Lovrinic 1984; Pickles 1988) have been of some concern, and to reduce spectral splatter at signal onset, signals are generally shaped with some finite rise time. The neglect of the physical parameters of sound onsets (other than the general concern about spectral splatter), despite the recognition that the initial discharges of most auditory neurons are evoked by stimulus onsets, has an almost paradoxical consequence: it can be seen in innumerable studies that measures of neuronal properties that were extracted from onset responses (or responses that contained an onset component) are reported and analyzed with respect to stimulus parameters that characterize features of the steady-state or plateau portion of the stimulus. An important case in point is the effect of sound pressure level (SPL) on neuronal onset responses. Alterations of the SPL of a stimulus inevitably coalter features of its onset, particularly when the rise function and the rise time are held constant, as is routinely done. When stimuli are shaped with the widely used linear rise function, for example, the most obvious feature is the slope of the envelope, i.e., the rate at which the peak pressure changes until the plateau value is reached. Any 6-dB increase in SPL will double this rate. A second feature that is coaltered with SPL under such conditions is the quasi-instantaneous acceleration of peak pressure, a parameter whose potential relevance has not been recognized at all. Both stimulus onset parameters are also coaltered when the rise time is altered and the SPL is held constant. Thus it is conceivable that neuronal onset responses might be shaped by factors other than the SPL or the short-term frequency spectrum.

Natural sound onsets will not only vary due to variation of signal SPL, but, because of differences in the manner in which sounds are produced, also due to variation in signal rise time (e.g., Cutting and Rosner 1974; Hall and Feng 1988). In speech sounds, for example, rise time can vary with the manner of articulation (Pickett 1980; Stevens 1980). Rise time can in fact cue perceptual categories in speech (Cutting and Rosner 1974; Stevens 1980), but clearly affects the perception of nonspeech sounds as well (Cutting and Rosner 1974). In humans, the just noticable difference for a change in rise time is ~25% of the duration of the rise time (van Heuven and van den Broecke 1979). Natural signals, including speech sounds, also differ in rise function, but according to our knowledge, in no physiological or psychophysical studies has the potential relevance of this onset feature been investigated. Nevertheless, the auditory system will experience, and may be able to discriminate, a wealth of different sound onsets.

In the present study and the companion paper (Heil 1997) the question of how auditory onset responses code or represent auditory onsets is investigated. This question is addressed by focusing the analysis on onset parameters such as the rate of change or the acceleration of peak pressure. Onset features were varied by varying SPL, rise time, and rise function. In addition to the widely used linear rise function, which is characterized by a constant rate of change of peak pressure during the rise time, cosine-squared rise functions were used. These have the advantage that peak pressure, rate of change, and acceleration of peak pressure are smooth and assessable functions of time that reach their maxima at different points during the rise time and are differentially affected by manipulations of rise time or SPL. Neurons of the primary auditory cortex (AI) are particularly suited to tackle the issue of onset coding because they preferentially respond to sound onsets, and any later discharges, if they occur, can be readily distinguished (e.g., Brugge et al. 1969). Because auditory cortical neurons have complex frequency filters, we have employed simple tonal stimuli to more easily decipher the effects of carrier frequency. A thorough understanding of coding strategies for isolated onsets will also promote our understanding of the coding of envelope transients that occur periodically or aperiodically during the course of complex auditory signals and that are so critical for speech recognition (Shannon et al. 1995). Preliminary reports of some of the findings have been presented (Heil 1996; Heil and Irvine 1996a).

METHODS

Animal preparation

Seven adult cats (3 females and 4 males, weighing between 2.6 and 3.8 kg) contributed data to this study. All had healthy ears as judged by otoscopic inspections of the tympani and middle ears and by the shapes and sensitivities of the N_1 audiogram. Each cat was deeply anesthetized with pentobarbitone sodium (40 mg/kg ip). Atropine (0.3 ml im) was administered to reduce tracheal mucous secretion. A broad-spectrum antibiotic (Amoxil; 0.5 ml im) was also given. The trachea and the radial vein were cannulated and anesthesia was maintained throughout surgery and recordings (up to 30 h) by intravenous injections of pentobarbitone in a physiological saline solution that also contained a few drops of heparin. The electrocardiogram was continuously monitored and rectal temperature was held near 38°C by a thermostatically controlled DC blanket. Surgical procedures have been described in detail elsewhere (Heil et al. 1992b). In brief, the left auditory cortex was exposed by trepanation of the overlying skull and removal of the dura. A specially designed Perspex chamber was mounted to the skull surrounding the opening, filled with warm saline, and sealed with a glass plate on which a small hydraulic microdrive was mounted and that housed the glass-insulated tungsten microelectrode. Each bulla was exposed and a round-window electrode and a length of fine-bore polyethylene tubing, allowing static pressure equalization within the middle ear, were inserted through a small hole. Thereafter the bullae were resealed with dental acrylic. The external meati were also cleared of surrounding tissue and transected to leave only short meatal stubs.

Acoustic stimulation and recording procedures

The cat was located in a sound-attenuating chamber. Stimuli were digitally produced (Tucker Davis Technology) and presented to the cat's ears via precalibrated sealed sound delivery systems. Each system consisted of a STAX SRS-MK3 transducer in a coupler. The sound delivery tube of the coupler fitted snugly into the meatal stub.

During viewing under an operating microscope, the microelectrode (tip diameter ~ 10 μm; impedances ~ 3–5 MΩ at 1 kHz) was positioned manually close above a chosen point on the cortical surface and was then advanced near-normal to the surface by means of the microdrive. Neural activity was amplified (×1,000) and, for recording of action potentials, also filtered (500–5,000 Hz) and displayed on storage oscilloscopes.

Once a neuron was well isolated, its characteristic frequency

(CF; frequency of lowest response threshold) and its preferred laterality of stimulus presentation (viz., monaural ipsilateral, monaural contralateral, or binaural with identical tones to each ear) were determined by manually varying the appropriate stimulus parameters. The discriminator level was set to trigger off either the positive or the negative slope of the filtered action potential waveform, but was not switched between the two during data acquisition. Adjustments of the trigger level during data acquisition were sometimes necessary. However, the effects of this procedure on the trigger instant were very small (<0.1 ms, as judged by inspection of the oscilloscope traces). Event times were stored on disk with 10-μs resolution for off-line analysis.

Under computer control, 20 repetitions of CF tones with a given rise function and a fixed rise time were presented at 1 Hz, at SPLs ranging from below threshold up to 90 dB SPL in 10-dB steps, followed by a measure of spontaneous activity. A different rise time was then selected and the recording procedure was repeated. As many as seven different rise times, covering the range of 1–170 ms, were tested and presented in random sequence. Most neurons were tested with CF tones of their preferred stimulus laterality, but some were tested with other stimulus lateralities and at other frequencies as well. In the latter cases, tones of a given rise function and rise time but of different frequencies and amplitudes were presented pseudorandomly as described in detail elsewhere (Heil et al. 1992b).

All tone bursts were 400 ms in duration including the times comprised by the symmetrical rise and fall functions. Tone bursts were shaped with either linear or cosine-squared rise and fall functions. Because it is the peak pressure *PP* (measured in Pa, and not the SPL, expressed in dB SPL), that changes according to the rise function, it is thus convenient for the present purpose to express the SPL as the plateau peak pressure PP_{plateau}.

With the cosine-squared rise function used here, peak pressure (in Pa) changes as a function of time t (in s) according to

$$PP = PP_{\text{plateau}} * \cos^2(t/CRT * \pi/2 + \pi/2) \quad \text{with} \quad 0 \le t \le CRT \quad (1)$$

where *CRT* is the cosine-squared rise time (in s).[1]

The rate of change of peak pressure *RCPP* (in Pa/s) varies with time according to

$$RCPP = -\pi/CRT * PP_{\text{plateau}} * \cos(t/CRT * \pi/2 + \pi/2) \times \sin(t/CRT * \pi/2 + \pi/2) \quad (2)$$

Maximum *RCPP* is reached halfway through the rise time and is given by

$$RCPP_{\max} = PP_{\text{plateau}}/2 * \pi/CRT \quad (3)$$

The acceleration of peak pressure *APP* (in Pa/s^2) varies with time according to

$$\begin{aligned} APP &= -(\pi/CRT)^2/2 * PP_{\text{plateau}} * [\cos^2(t/CRT * \pi/2 + \pi/2) \\ &\quad - \sin^2(t/CRT * \pi/2 + \pi/2)] \\ &= -(\pi/CRT)^2/2 * PP_{\text{plateau}} * \cos(2\pi * t/CRT + \pi) \end{aligned} \quad (4)$$

Maximum *APP* occurs at the beginning of the rise time and is given by

$$APP_{\max} = PP_{\text{plateau}}/2 * (\pi/CRT)^2 \quad (5)$$

With a linear rise function, the peak pressure changes according to

$$PP = PP_{\text{plateau}} * t/LRT \quad \text{with} \quad 0 \le t \le LRT \quad (6)$$

where *LRT* is the linear rise time (in s) and PP_{plateau}/LRT identifies the constant rate of change of peak pressure *RCPP* (in Pa/s). Mathematically, acceleration and deceleration of peak pressure are instantaneous and infinite and occur at the beginning and at the end of the rise time, respectively.

The time courses of peak pressure, rate of change, and acceleration of peak pressure for cosine-squared and for linear rise functions are schematically illustrated in Figs. 1 and 9, respectively.

Data analysis

Spikes in response to the 20 presentations of a given stimulus were displayed off-line as a poststimulus time histogram. The histogram was used to select analysis windows that would comprise only onset responses and would discard late discharges, offset responses, and occasionally presumed spontaneous spikes. Spontaneous activity was generally very low (<3 spikes/s) and late discharges, if they occurred at all, were clearly separated in time from onset responses by marked intervals of no activity. Thus the selection of an appropriate onset window was generally straightforward. In most cases, analysis windows used for a given neuron were the same for all rise times and amplitudes studied (e.g., from 5 to 100 ms after tone burst onset). In some instances, however, different windows had to be selected. In these cases, windows for tones of long rise times and low amplitudes were longer or delayed relative to windows for tones of short rise times and high amplitudes, because otherwise onset responses would have been missed or late responses would have been included, respectively. In the present paper aspects of spike timing are analyzed, whereas in the companion report the focus is on response magnitudes. Only the timing of the first (and in many neurons the only) spike will be considered because the interspike intervals of the onset responses of auditory cortex neurons, which discharge more than one spike per stimulus, are very regular and independent of stimulus level (Phillips and Sark 1991). Mean and SD of first-spike latency, measured from stimulus onset, response probability, and number of discharges in the window were computed. As a rule, only means and SDs based on response probabilities of ≥0.15 were considered further.

RESULTS

The results on mean first-spike latency are presented first, and then those on the variability of first-spike latency. In each section, data recorded with cosine-squared rise function tones are presented before those recorded with linear rise function tones, followed by a comparison of the results obtained with the two different rise functions.

Data base

This study is based on 74 well-isolated single neurons, recorded in the left AI, as inferred from the locations of the recording sites with respect to the sulcal pattern, the tonotopic sequence, and the presence of a short-latency strong evoked potential to tone bursts. In only one penetration in one cat did we not see an AI-like evoked potential. The two neurons recorded in this penetration (*95-87/03* and *95-87/04*) had very long minimum latencies (>30 ms). A few isolated AI neurons, which were spontaneously active, appeared not to be driven by tone bursts. Sixty-five neurons were studied with tones shaped with cosine-squared rise functions, 39 neurons were studied with tone bursts shaped with linear rise functions, and 30 neurons were studied with both types of tones. Tones were presented with the neuron's preferred stimulus laterality, which was binaural for 31 neurons, con-

[1] Tucker Davis Technologies utilizes a fudge factor of 0.5903 in their built-in cosine-squared rise function so that the actual rise time is 1.69 times as long as the one specified by the experimenter.

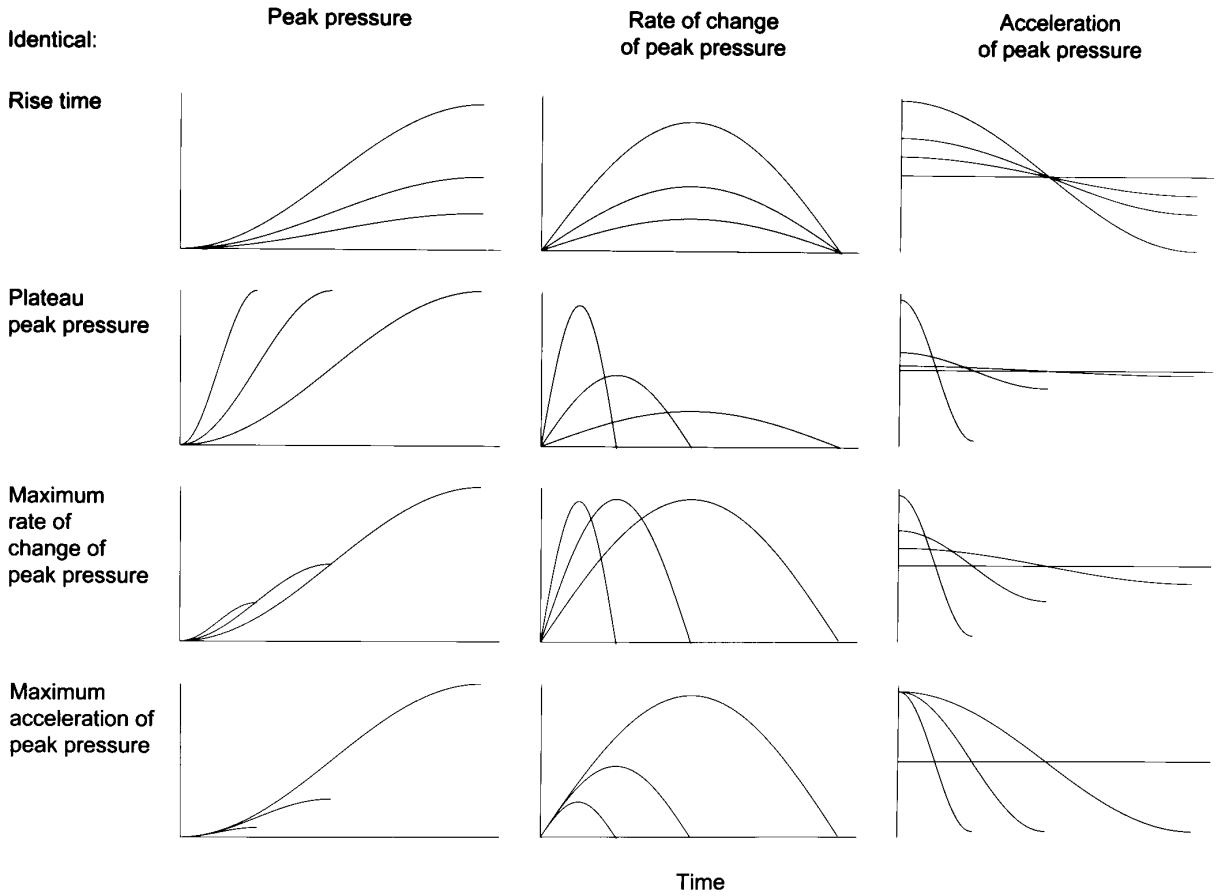

FIG. 1. Schematics of envelope characteristics of the onsets of tone bursts shaped with cosine-squared rise functions. *Left*: for 3 different stimuli, time courses of the peak pressure during the rise time are shown. Only the top halves of the symmetrical envelopes are illustrated. *Middle* and *right*: resulting time courses of the rate of change of peak pressure and the acceleration of peak pressure, respectively. Signals in the rows from *top* to *bottom* are of identical rise time, plateau peak pressure, maximum rate of change of peak pressure, and maximum acceleration of peak pressure, respectively. Note that plateau peak pressure, rate of change of peak pressure, and acceleration of peak pressure reach their maxima at different points during the rise time.

tralateral for 40 neurons, and ipsilateral for 3 neurons. Four neurons were in addition studied with several stimulus lateralities. The neurons in the sample had CFs ranging from 1.5 to 35.2 kHz, with most CFs in the octave band from 12 to 24 kHz. Three neurons were also studied at multiple frequencies other than their CFs.

Mean first-spike timing

ASPECTS OF COSINE-SQUARED RISE FUNCTION TONES. Figure 1, *left*, schematically illustrates the time courses of the envelopes of the onsets of cosine-squared rise function signals. During the rise time the peak pressure (in Pa), but not the SPL (in dB SPL), of the signal changes according to the rise function (Fig. 1, *top left*). The rate of change of peak pressure also changes gradually during the rise time (Fig. 1, *top middle*). It is zero at the beginning and at the end of the rise time and reaches a maximum halfway through the rise time. Acceleration of peak pressure is maximal at the beginning of the rise time and decreases smoothly with time. It is zero halfway through the rise time. From then on acceleration becomes increasingly negative (deceleration) and reaches a negative maximum at the end of the rise time (Fig. 1, *top right*). Thereafter acceleration is zero. Alterations of both plateau peak pressure and rise time effect the onset of stimuli shaped with cosine-squared rise functions, but in different fashions. A 6-dB increase in the plateau SPL of stimuli with a given rise time will lead to a twofold increase in the maximum rate of change of peak pressure and in the maximum acceleration of peak pressure. Shortening the rise time by a factor of 2 for any given plateau SPL also leads to a twofold increase in the maximum rate of change of peak pressure (Fig. 1, *2nd row, middle*), but maximum acceleration of peak pressure increases fourfold (Fig. 1, *2nd row, right*). Therefore signals can be grouped to match in rise time, plateau peak pressure, maximum rate of change of peak pressure, or maximum acceleration of peak pressure (Fig. 1, *1st–4th rows*, respectively). Signals that share the same value of maximum acceleration of peak pressure differ in rise time and in plateau peak pressure (Fig. 1, *bottom row*).

MEAN FIRST-SPIKE LATENCY TO COSINE-SQUARED RISE FUNCTION TONES. Figure 2*a* shows the mean first spike latencies of one AI neuron (*95-95/04*) to contralateral CF tone bursts of 22 kHz, all shaped with cosine-squared rise functions. The data are plotted as a function of plateau peak pressure

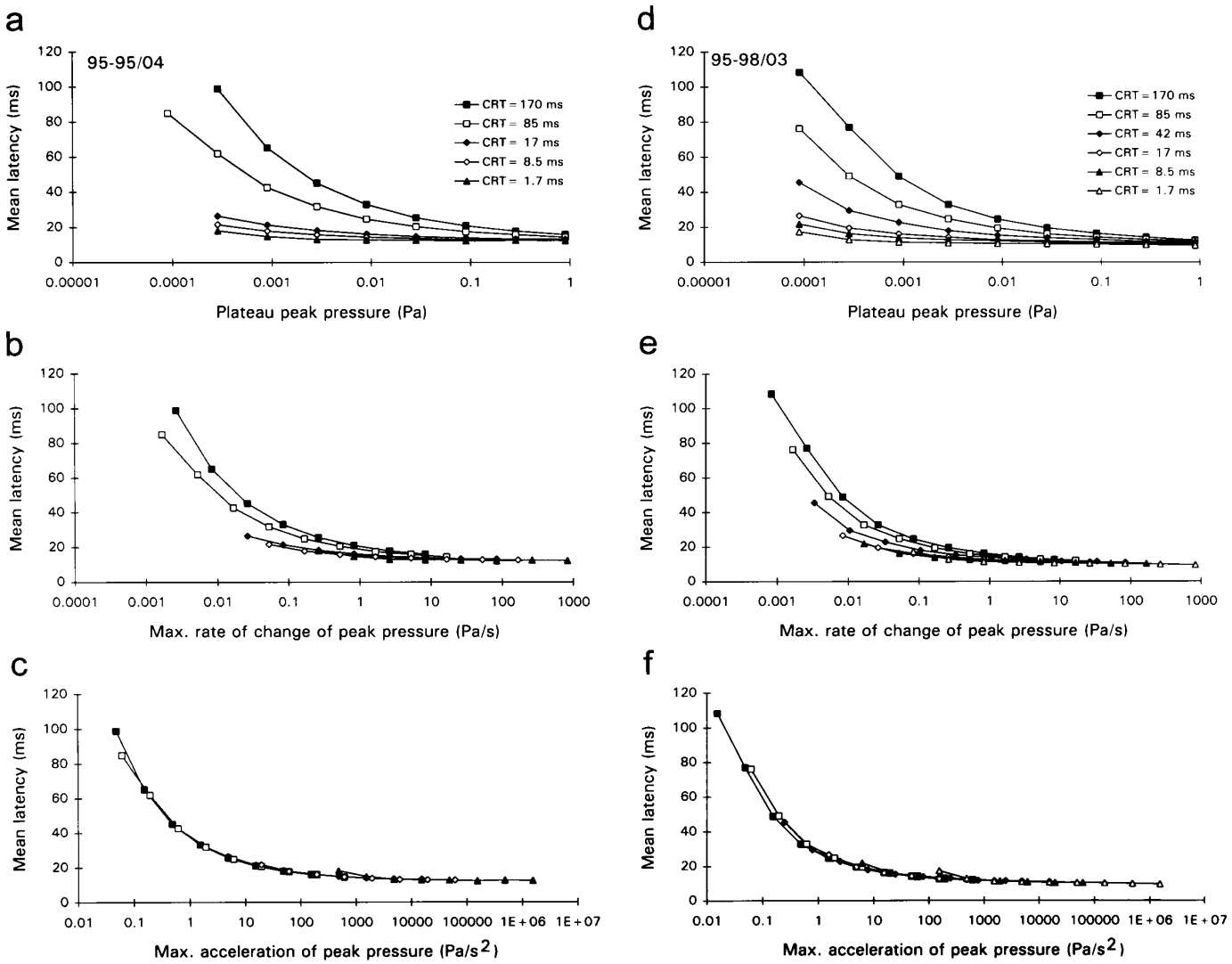

FIG. 2. Effects of rise time and plateau peak pressure of cosine-squared rise function tones on latency. Mean 1st-spike latency of *neurons 95-95/04* and *95-98/03* (*left* and *right*, respectively) to 20 repetitions of characteristic frequency (CF) tones shaped with cosine-squared rise functions of 5 and 6 different rise times (see key). In *a* and *d*, mean latency is plotted as a function of plateau peak pressure (in Pa). The range of 5 orders of magnitude is equivalent to a 100-dB range of sound pressure level (SPL) from about −10 to 90 dB SPL. In *b* and *e*, mean latency is plotted as a function of the maximum rate of change of peak pressure, and in *c* and *f* as a function of the maximum acceleration of peak pressure. Note the close congruence of the latency-acceleration functions. For further details see RESULTS.

(in Pa). The longest mean first-spike latency of ~100 ms was measured in response to tones with 170-ms rise times and plateau peak pressures of 0.00028 Pa, equivalent to 20 dB SPL. For each rise time, latency declines nonlinearly with increasing plateau peak pressure. For tones of any given plateau peak pressure, latency increases systematically with rise time, although the different functions appear to converge on a single minimum at ~12.3 ms.

Similar observations can be made when latency is plotted as a function of the maximum rate of change of peak pressure (Fig. 2*b*). Although the functions relating latency to maximum rate of change of peak pressure obtained with different rise times are closer together than those relating latency to plateau peak pressure, latency still increases with rise time for signals with the same maximum rate of change of peak pressure. Also, for some tones of long rise time the neuron discharges before the maximum rate of change of peak pressure is reached.

In contrast, when latency is plotted as a function of maximum acceleration of peak pressure, all five latency-acceleration functions obtained with different rise times are in close register, i.e., at any given acceleration the functions are within 1 SD of the means (Fig. 2*c*). For clarity, SDs are not plotted in Fig. 2, but decreased for *neuron 95-95/04* from 6.4 to 0.5 ms.

Tones with a common maximum acceleration at their onsets also share a number of other properties. These are the maximum deceleration occurring at the end of the rise time; the mean acceleration and mean deceleration averaged over the first and second half of the rise time, respectively; the ratio of $RCPP_{max}$ and rise time; and the ratio of $PP_{plateau}$ and the square of the rise time (Fig. 1; *Eq. 4* and *5*). However,

these parameters or any combination thereof can be ruled out as determinants of latency because in response to many tones, particularly of long rise times, the first spike occurs long before the end, or even the midpoint, of the rise time (Fig. 2).

Data from a second neuron (*95-98/03*) are illustrated in Fig. 2, *d–f*. This neuron's CF was similar to that of *95-95/04* (viz., 21 kHz), but the neuron was excited best by tones presented to the ipsilateral ear. The total range of latencies obtained with the six different rise times tested was nearly 100 ms. As was the case for *neuron 95-95/04*, all latency functions obtained with different rise times were in close register only when plotted as a function of the acceleration of peak pressure (Fig. 2*f*).

In all 65 neurons studied with cosine-squared rise function tones, mean latencies obtained at any given acceleration of peak pressure with tones of different rise times were within 1 SD of each other. Note that over the range of rise times used (1.7–170 ms), tones with the same maximum acceleration differ in plateau peak pressure by as much as 80 dB, i.e., by a factor of 10,000.

In several cases, some mean latencies could be systematically longer than others recorded to tones of the same maximum acceleration of peak pressure. In all these cases, the extraordinarily long latencies were measured to tones closest to the firing threshold of the neuron (e.g., the mean latencies to the 1.7-ms rise time tones with accelerations between 100 and 1,000 Pa/s^2 in Fig. 2, *c* and *f*). *Neuron 95-98/14* (Fig. 14*a*) represents the most drastic example of this ''near-threshold effect.'' In this case the means of first-spike latency closest to threshold are based on the same response probability (viz., 100%) as are all the other means. In other cases in which the near-threshold effect was observed, the exceptionally long near-threshold means were mostly based on much lower response probabilities (e.g., *neuron 95-98/08* in Fig. 3*a*).

Latency-acceleration functions obtained with shorter rise times take up the common course of the latency-acceleration functions obtained with longer rise times at consecutively higher values of maximum acceleration of peak pressure (e.g., Figs. 2, 3, and 13, *a* and *d*). Thus a neuron's firing threshold is not determined by the maximum acceleration of peak pressure at signal onset (see also companion paper).

COMPARISON OF LATENCY-ACCELERATION FUNCTIONS AMONG DIFFERENT NEURONS. The latencies of *neurons 95-95/04* and *95-98/03* in Fig. 2 are plotted with the same resolution, and comparison of Fig. 2, *c* and *f*, reveals that their latency-acceleration functions are very similar in shape. In Fig. 3*a*, latency-acceleration functions obtained from another five neurons are plotted in a single graph, facilitating a comparison of latency-acceleration functions among different neurons. The data illustrated in Fig. 3*a* were selected to represent neurons recorded in different cats and with widely different CFs (range 2.3–30 kHz), data obtained with different laterality of presentation, and functions covering very different ranges of latency. The latency-acceleration function of *neuron 95-98/08* (◆) covered an extensive range of latency (130–15 ms) and of maximum acceleration of peak pressure (>8 orders of magnitude). Because of higher response thresholds, strongly nonmonotonic spike count functions, or both, the latency-acceleration functions of the other neurons were more restricted along the abscissa, but also along the ordinate. However, an inspection of Fig. 3*a* suggests that the shapes of these more restricted functions closely resemble sectors of the extensive function of *neuron 95-98/08*. This is most obvious for *neuron 95-95/03* (○), which had a threshold slightly higher than that of *neuron 95-98/08*. *Neuron 95-92/21* (▲) had a considerably higher threshold, but also slightly longer mean latencies, than *neuron 95-98/08*. But even the course of the latency-acceleration function of *neuron 95-98/16* (●), which is restricted at each end, resembles the course of the extensive function of *neuron 95-98/08* in its intermediate part.

All 93 latency-acceleration functions, obtained from the 65 neurons studied with cosine-squared rise functions tones, had strikingly similar shapes. All functions could be brought into very close register by allowing them to be shifted only along the ordinate and along the abscissa, as initially judged by visual inspection. Shifts along the ordinate compensate for differences in the minimum or asymptotic latency, and shifts along the abscissa compensate for differences in sensitivity to acceleration.

MATHEMATICAL DESCRIPTION OF LATENCY-ACCELERATION FUNCTIONS. To get quantitative measures of the similarity of the latency-acceleration functions of different neurons and of the shifts along the ordinate and abscissa required to obtain congruence, a simple mathematical function was selected that described the form of the latency-acceleration functions, and also allowed quantification of the positional differences along the abscissa and the ordinate

$$L_{CRF} = L_{min} + A_{CRF} * (\log APP_{max} + S)^{-\alpha} \quad (7)$$

The subscript CRF indicates that the measures were obtained with cosine-squared rise function tones. L_{CRF} is a neuron's mean latency as a function of maximum acceleration of peak pressure APP_{max}. L_{min} is the minimum or asymptotic latency against which L_{CRF} converges for acceleration approaching infinity. L_{min} is a constant that would include all the delays that are independent of the stimulus magnitude, such as acoustic delays, delays introduced by the traveling wave in the cochlea, the sum of all axonal travel times, and possibly some synaptic factors. The other term describes the inverse dependence of latency on the magnitude of maximum acceleration of peak pressure, where A_{CRF} is a scaling factor and S is the neuron's transient sensitivity, which codetermines the position of the function along the abscissa. The value of S is the logarithm of an acceleration of peak pressure (in Pa/s^2). A larger S places the function more to the left and represents a higher transient sensitivity (see also Fig. 3*b*). The function does not account for the near-threshold effects observed in some neurons and described above. It also does not account for the finding that in a few neurons with nonmonotonic spike-count functions, mean latency could increase slightly but systematically with very high values of maximum acceleration of peak pressure (e.g., *95-95/03* in Fig. 3, *a* and *b*).

Iterative curve fitting was performed in the following way. In initial fitting procedures, L_{min}, A_{CRF}, S, and the exponent α were allowed to vary. Each deviation of the fitted function from the measured mean latency was squared and then weighted by multiplying it with the response probability on

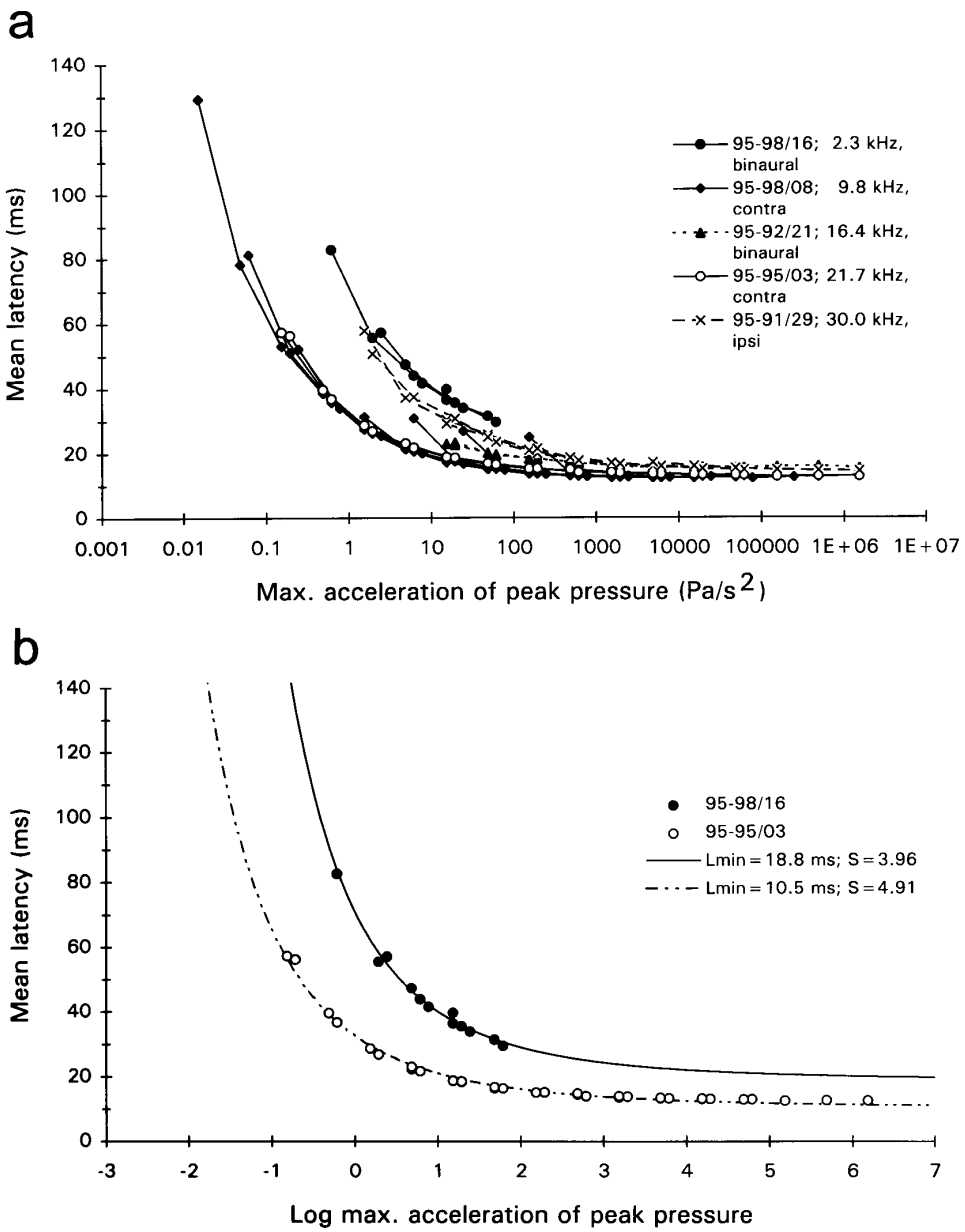

FIG. 3. Comparison of latency-acceleration functions. *a*: data from neurons from different cats, with different CFs, obtained with different laterality of stimulus presentation are selected to illustrate the similarity in the shapes of the latency-acceleration functions despite differences in their extent. Mean latencies obtained from a given neuron are represented by the same symbols, and latencies obtained from that neuron with tones of the same rise time are connected by solid lines. Note that, as in the cases illustrated in Fig. 2, mean latencies are in close register when plotted as a function of maximum acceleration of peak pressure. *b*: mean latencies of 2 neurons from *a* are reproduced. Solid and dashed lines: best fits of *Eq. 8* to the data. The 2 fitted functions have identical shape. As can be derived from the differences in the solutions for L_{min} and S for the 2 neurons (as specified in the key), the function for *neuron 95-98/16* is displaced upward by 8.3 ms and rightward by 0.95 log units of maximum acceleration of peak pressure relative to the function of *neuron 95-95/03*. For further descriptions see RESULTS.

which the measured mean was based. The smallest sum of the weighted squared deviations, i.e., the best fit, was generally found with <1,000 iterations. In some cases the fit was found to improve with increasing α. The improvement, however, was marginal for $\alpha > 4$, and also pushed A_{CRF} into unwieldy dimensions (e.g., years for $\alpha = 10$). For a second fitting step, we therefore selected $\alpha = 4$, and allowed L_{min}, A_{CRF}, and S to vary. For the 93 different functions fitted, A_{CRF} showed a unimodal distribution. Figure 4*a* shows a scatterplot of A_{CRF} against the number of first spikes that had contributed to the fitted function. The figure shows that the width of the distribution of A_{CRF} diminished rapidly with increasing number of first spikes and converged toward the weighted average of $\tilde{A}_{CRF}$ = 12,791 ms (Fig. 4*a*, – – –). In a third and final fitting procedure, A_{CRF} was also kept constant (at 12,791 ms). In this way, a function with a fixed shape, as determined by α and A_{CRF}, but free to be placed within the coordinate system of latency and maximum acceleration of peak pressure, was fitted to the data

$$L_{CRF} = L_{min} + \tilde{A}_{CRF} * (\log APP_{max} + S)^{-4} \quad (8)$$

Figure 4*b* provides a scatterplot of the sums of the weighted least-squared deviations of mean latency obtained with the second and third fitting step, i.e., with A_{CRF} variable and $\tilde{A}_{CRF}$ fixed at 12,791 ms, respectively. Only few points are considerably above the line of unity slope (dashed line). The three most deviating points were provided by one neuron tested under different stimulus conditions. In general, the most deviating points were based on low numbers of first spikes. Most points are in relatively close proximity to the dashed line, indicating that the latency-acceleration function with the fixed shape provides nearly as good a description of the data as does a function with an additional free variable.

In Fig. 3*b*, the mean latencies of two of the neurons

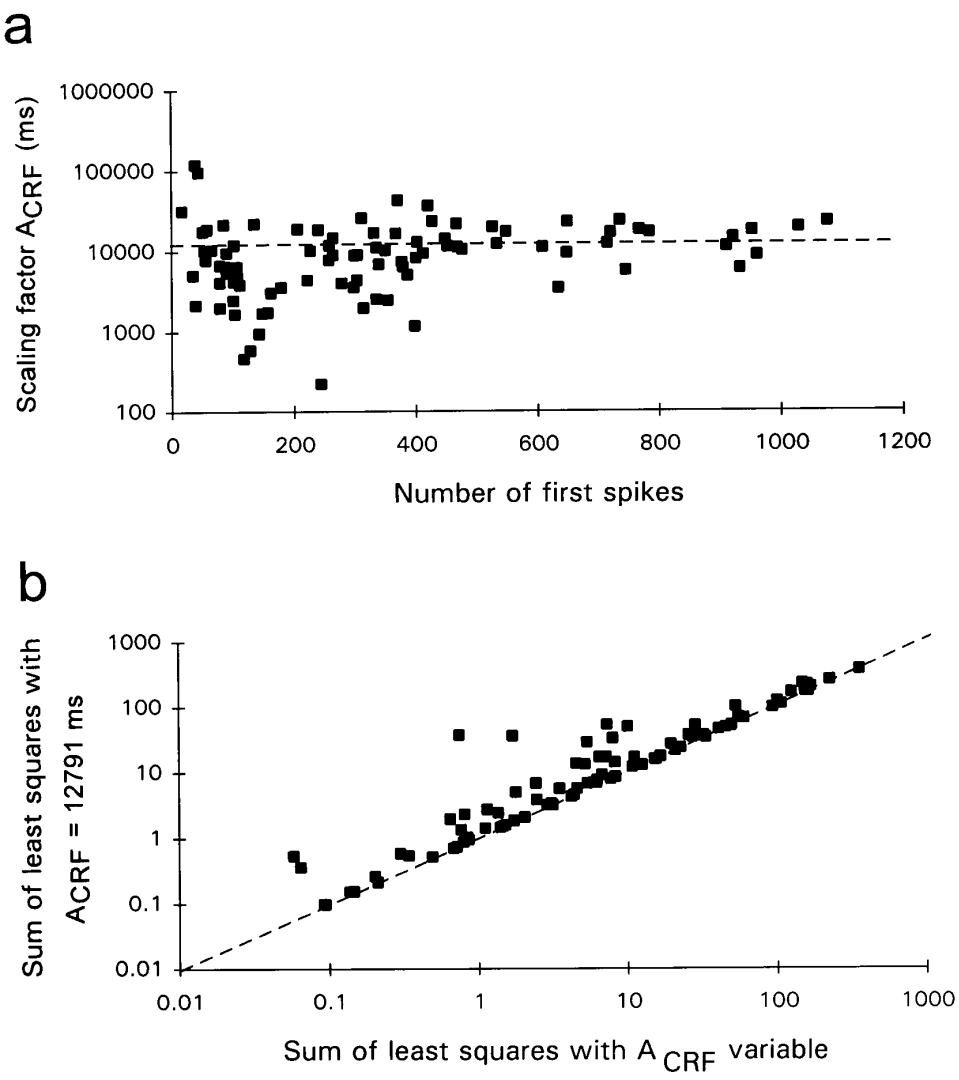

FIG. 4. Descriptions of neuronal latency-acceleration functions. *a*: scatterplot of the scaling factor A_{CRF} obtained from fitting the function

$$L_{CRF} = L_{min} + A_{CRF} * (\log APP_{max} + S)^{-4}$$

to neuronal latency-acceleration functions against the number of 1st spikes contributing to the fit. Note that the distribution converges against the weighted average of $\tilde{A}_{CRF}$ = 12,791 ms (– – –) with increasing number of 1st spikes, thus with presumed increasing reliability of the fit. *b*: scatterplot of the sums of the weighted least-squared deviations of the above functions, fitted to the relationship between mean latency and maximum acceleration of peak pressure, from the actual data. A_{CRF} was either a free parameter or it was fixed at $\tilde{A}_{CRF}$ = 12,791 ms, the value of its weighted average. In only a few instances was the quality of the fit notably reduced when A_{CRF} was fixed. Note that most points are close to the line of unity slope (– – –).

of Fig. 3*a* (viz., *95-95/03* and *95-98/16*) are reproduced together with the fitted functions (*Eq. 8*), which are of identical shape. The figure allows a visual assessment of the quality of the fit and the similarity of the fitted function with neuronal latency-acceleration functions. The best solutions for *S* and L_{min} found by the final fitting procedure are 3.96 and 18.8 ms for *neuron 95-98/16* and 4.91 and 10.5 ms for *neuron 95-95/03*. Thus, according to the fitting results, the latency-acceleration function of *neuron 95-98/16* is displaced upward by 8.3 ms and rightward by 0.95 log units of acceleration relative to the function of *neuron 95-95/03*.

COMPARISON OF TRANSIENT SENSITIVITY AND FIRING THRESHOLD. *S* is not to be confused with firing threshold, a measure generally expressed in dB SPL and related to peak pressure. To emphasize this point more clearly, note, for example, that in Fig. 3*a*, the latency functions of *neurons 95-98/08* (♦) and *95-95/03* (○) are in nearly perfect register, without requiring any notable shifts to obtain congruence, i.e., the two neurons have the same *S*. However, the latency functions do not start at the same point along the abscissa, reflecting differences in their firing thresholds. Figure 5 presents, for all neurons in the sample, a scatterplot of the firing thresholds (in dB SPL) against *S*. Each neuron contributed multiple data points to the plot, because threshold SPL increased with rise time (see companion paper and also Fig. 6). Although a low transient sensitivity seems to exclude low-threshold SPLs, there is only a loose relationship between the two parameters (r^2 = 0.123; n = 319). Threshold SPLs can vary over a range of ≥100 dB for the same *S*.

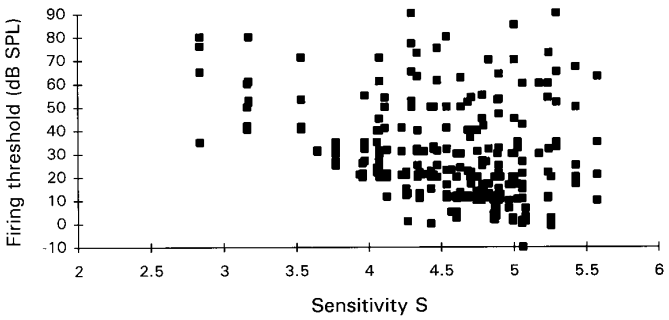

FIG. 5. Scatterplot of neuronal firing thresholds (expressed in dB SPL) against *S* extracted from latency-acceleration functions. *S* is the logarithm of acceleration of peak pressure measured in Pa/s^2. Note that the 2 measures are only loosely related.

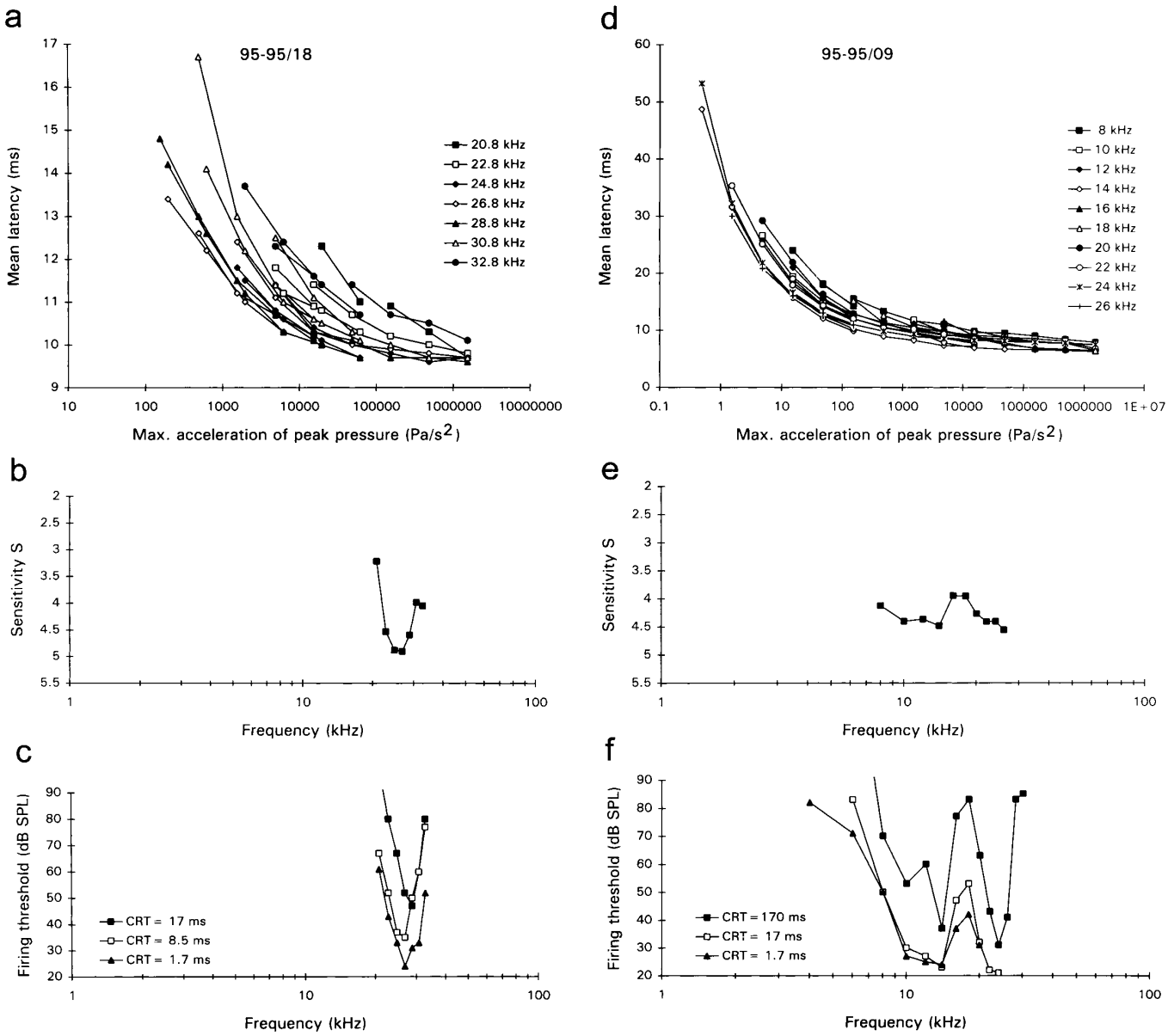

FIG. 6. Effects of tone burst frequency on latency-acceleration functions. Data from 2 neurons (*95-95/18*, *a–c*, and *95-95/09*, *d–f*) are shown. In *a* and *d*, mean latency is plotted against maximum acceleration of peak pressure and different symbols identify different frequencies. Mean latencies obtained with tones of the same cosine-squared rise time are connected. Note the different resolutions of the abscissas and ordinates in *a* and *d*. *b* and *e*: measure of *S*, obtained from fitting *Eq. 8* to the latency-acceleration functions for tones of different frequencies. *S* reflects the size of the lateral displacement of these functions, and a difference in *S* of 1 is equivalent to 20 dB. *c* and *f*: conventional response threshold curves or tuning curves obtained with tones of different cosine-squared rise times. Threshold was defined by a response probability of 0.1. Note the increase in thresholds with rise time throughout the frequency range (see also companion paper). Note that the transient sensitivity vs. frequency functions share features with the classical tuning curves (cf. *b* with *c* and *e* with *f*).

EFFECTS OF STIMULUS LATERALITY ON LATENCY-ACCELERATION FUNCTIONS. In four neurons latencies to tone bursts were presented with different stimulus lateralities, i.e., binaural, monaural contralateral, and monaural ipsilateral. In general, stimulus laterality had a very small, if any, effect on the shapes of the latency-acceleration functions or their horizontal position within the coordinate systems. In a comparison of stimulus laterality in a given neuron, fitting results yielded differences in *S* that averaged 0.1 and were all <0.3, $\sim 1/10$ of the variation seen across neurons. The largest effect of stimulus laterality was on the estimated L_{min}. With monaural ipsilateral stimulation L_{min} was consistently 2–3 ms longer than with contralateral or binaural stimulation, whereas differences in L_{min} between monaural contralateral and binaural stimulation were <0.9 ms.

EFFECTS OF STIMULUS FREQUENCY ON LATENCY-ACCELERATION FUNCTIONS IN A GIVEN NEURON. In three neurons latencies were obtained to tone bursts of different frequencies including the CF. Results from two of these neurons (*95-95/18* and *95-95/09*) are illustrated in Fig. 6. Figure 6,

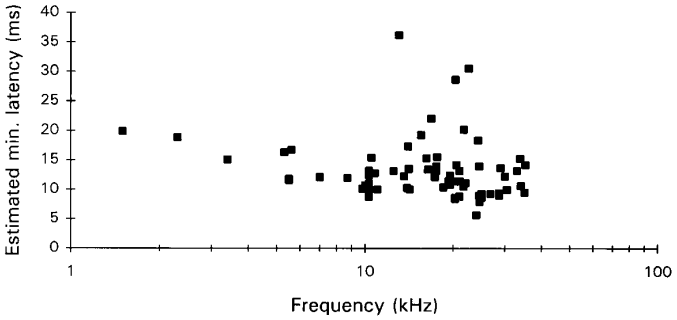

FIG. 7. Estimated minimum latency L_{min} obtained from fits of *Eq. 8* to the latency-acceleration functions plotted against tone frequency. Data obtained at frequencies other than the CF are omitted. Note that neurons of the same CF can differ widely in their minimum latency and that L_{min} tends to decrease with frequency.

a and *d*, shows mean latencies plotted against maximum acceleration of peak pressure. The latency-acceleration functions for different frequencies all have similar shape, but are obviously dispersed along the abscissa. The analysis of the fitting results illustrates the systematic nature of this dispersion: in Fig. 6, *b* and *e*, the value of *S* obtained from these fits is plotted against tone burst frequency. For *neuron 95-95/18* the highest transient sensitivity is obtained for 26.8 and 24.8 kHz, and *S* decreases toward higher and lower frequencies, whereas for *neuron 95-95/09* the function is more complex.

The transient sensitivity versus frequency functions can be compared with the more conventional threshold or tuning curves based on firing probabilities (Fig. 6, *c* and *f*). Tones of the same rise time that differ in peak pressure by 20 dB SPL differ in the acceleration of peak pressure by a factor of 10. This is equivalent to a difference in *S* of 1, so that the ordinates in Fig. 6, *b* and *c* and *e* and *f*, have the same relative scaling. The CF of *neuron 95-95/18* was near 26.8 kHz when tone bursts with 1.7- and 8.5-ms rise time were used, but shifted to 28.8 kHz with tone bursts having 17-ms rise times. In addition, with prolongation of the rise time systematic elevations in response threshold were observed throughout the excitatory frequency range, when threshold was expressed as a function of the plateau peak pressure or level (in dB SPL; Fig. 6*c*, see also companion paper). *Neuron 95-95/09* had twin-peaked tuning curves with lowest thresholds at 24 and at 14 kHz. Again, threshold SPLs increased systematically with rise time at all frequencies, although not by identical amounts (Fig. 6*f*). Note that the transient sensitivity versus frequency curves obtained from the analysis of latency-acceleration functions and the tuning curves share common features, but are not identical. For *neuron 95-95/09*, *S* and the tuning curves show a dip at 18 kHz (cf. Figs. 6, *e* and *f*), but this dip is more pronounced in the tuning curves, particularly those obtained with longer rise times.

For *neuron 95-95/18*, the estimated values of L_{min} obtained from the fits of the latency-acceleration functions varied between 8 and 9 ms and were not systematically related to frequency, whereas for *neuron 95-95/09*, L_{min} varied between ~4.5 and 7 ms with frequency, and its course approximately paralleled the tuning curve, with L_{min} being shortest at 14 and 26 kHz (not shown).

EFFECTS OF STIMULUS FREQUENCY ON LATENCY-ACCELERATION FUNCTIONS ACROSS NEURONS. For a comparison of latency-acceleration functions among different neurons, only measures obtained at CF were considered. Figure 7 provides a scatterplot of L_{min}, as obtained from the fits, against frequency. In different neurons, L_{min} varied between 5.6 and 37 ms, with most values between 9 and 15 ms. On average, L_{min} decreased with increasing CF. This decrease is obvious for the shortest L_{min} and a similar trend for the entire data set emerged from a regression analysis. L_{min} was closely correlated with the shortest measured latency ($r^2 = 0.894$), but on average was 1.8 ms shorter.

Figure 8 shows a scatterplot of *S* obtained from the fits over frequency. The least reliable *S* estimates are shown by open squares. The degree of reliability of *S* was quantified by the increase in the sum of the weighted least-squared deviations, when *S* was arbitrarily incremented by 1 after the best fit had been obtained. This increase could be as small as twofold, indicating low reliability for the obtained value of *S*, and as high as 1,200-fold, with a mean of 60-fold. For the open squares, the increase was <15-fold. The distribution of *S*, particularly that of the most reliable measures (solid squares), is similar to the cat's compound action potential audiogram. The audiogram shows highest sensitivity at ~10 kHz, and a steeper rolloff for higher than for lower frequencies (see Rajan et al. 1991 for illustrations of audiograms measured under different stimulus conditions). At most frequencies the vertical scatter in the data points of Fig. 8 is in the range of only 0.5, equivalent to 10 dB. Because there may have been differences in hearing sensitivity among the six cats that contributed data to this figure, differences in the sensitivities of the two ears in a given cat, and imprecisions in CF determination (cf. Fig. 6), it is conceivable that some, if not all, of this vertical scatter may be noise due to these factors.

ASPECTS OF LINEAR RISE FUNCTION TONES. With linear rise functions, the rate of change of peak pressure during the rise time is constant (Fig. 9) and, for a given rise time, its magnitude is directly proportional to the plateau peak pressure achieved at the end of the rise time, and, for a given plateau peak pressure, is inversely proportional to rise time. Thus the first derivative of the stimulus envelope has the shape of a rectangle, with its vertical axis proportional to rate of change of peak pressure (expressed in Pa/s) and its horizontal axis equivalent to the rise time (Fig. 9, *middle*).

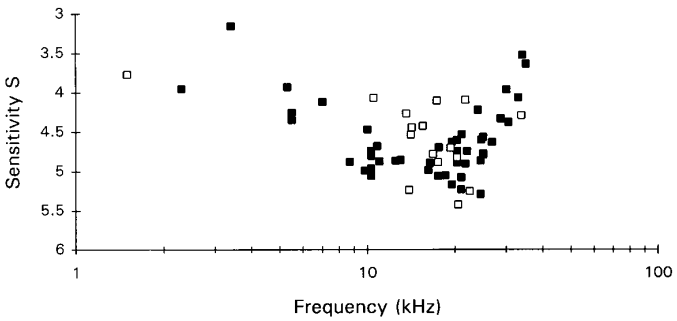

FIG. 8. *S* obtained from fits of *Eq. 8* to the latency-acceleration functions plotted against tone frequency. Data obtained at frequencies other than the CF are omitted and fits with the most reliable *S* are shown with solid squares.

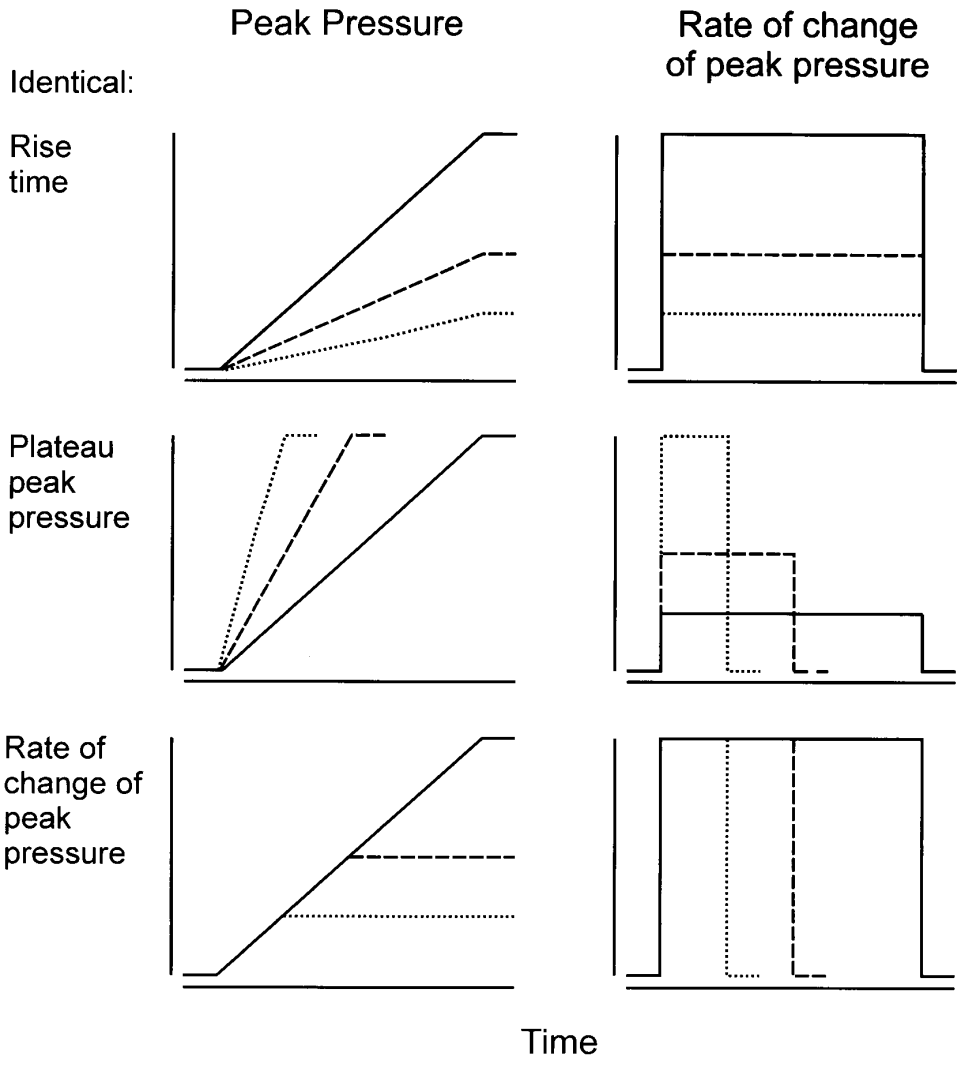

FIG. 9. Schematics of envelope characteristics of the onsets of tone bursts shaped with linear rise functions. *Left* and *right*: for 3 different stimuli (identified by ——, – – –, and · · ·), the time courses of peak pressure and of rate of change of peak pressure, respectively. Signals in the *top row* are of identical rise time, signals in the *middle row* are of identical plateau peak pressure, and signals in the *bottom row* are of identical magnitude of rate of change of peak pressure.

Signals shaped with linear rise functions can be grouped to match either in rise time (Fig. 9, *top*), in plateau peak pressure (*middle*), or in the rate of change of peak pressure (*bottom*). Acceleration of peak pressure occurs at the beginning of the rise time and deceleration occurs at the end of the rise time. Mathematically, acceleration and deceleration are instantaneous and their magnitudes are infinite.

MEAN FIRST-SPIKE TIMING TO LINEAR RISE FUNCTION TONES. Figure 10, *a* and *b*, shows the mean first-spike latencies of *neuron 95-95/04* to linear rise function tones. It is the same neuron for which latencies obtained with cosine-squared rise function tones were illustrated in Fig. 2, *a–c*. Figure 10*a* illustrates that for each rise time, latency declines nonlinearly with plateau peak pressure. For tones of a given plateau peak pressure, latency increases with rise time. As was the case with cosine-squared rise function tones, the curves appear to converge on a single minimum and in response to some tones of long rise times the neuron discharges long before the plateau peak pressure is reached.

Figure 10*b* shows mean first spike latencies plotted over the rate of change of peak pressure during the rise time. Note that all five functions are now in very close register, i.e., for any given rate of change of peak pressure, mean latencies are within <1 SD of each other.

A second example (*neuron 95-87/13*) is illustrated in Fig. 10, *c* and *d*. This neuron had a CF similar to that of *neuron 95-95/04* (viz., 20.5 kHz), but was stimulated binaurally and had a much more restricted range of latencies ($\sim$12–18 ms).

In all 39 neurons studied with linear rise function tones, tone bursts characterized by the same rate of change of peak pressure during the rise times elicited a response from a given neuron with the same first-spike latency, i.e., within 1 SD of the mean, irrespective of differences in rise time or plateau peak pressure. Tones of identical rate of change of peak pressure that differ in rise times by a factor of 100 differ in plateau peak pressure by the same factor, i.e., by 40 dB. The finding that tones with rise times of 1–100 ms and possibly beyond those limits initiate spikes with the same latency, provided they have identical rate of change of peak pressure, suggests that the latency of the first spike must be determined very early during the rise time, viz., within <1 ms after stimulus onset.

POST HOC ANALYSIS OF PREVIOUSLY PUBLISHED LATENCY DATA. There has been one previous report on the effect of varying rise time and level of linear rise function tones

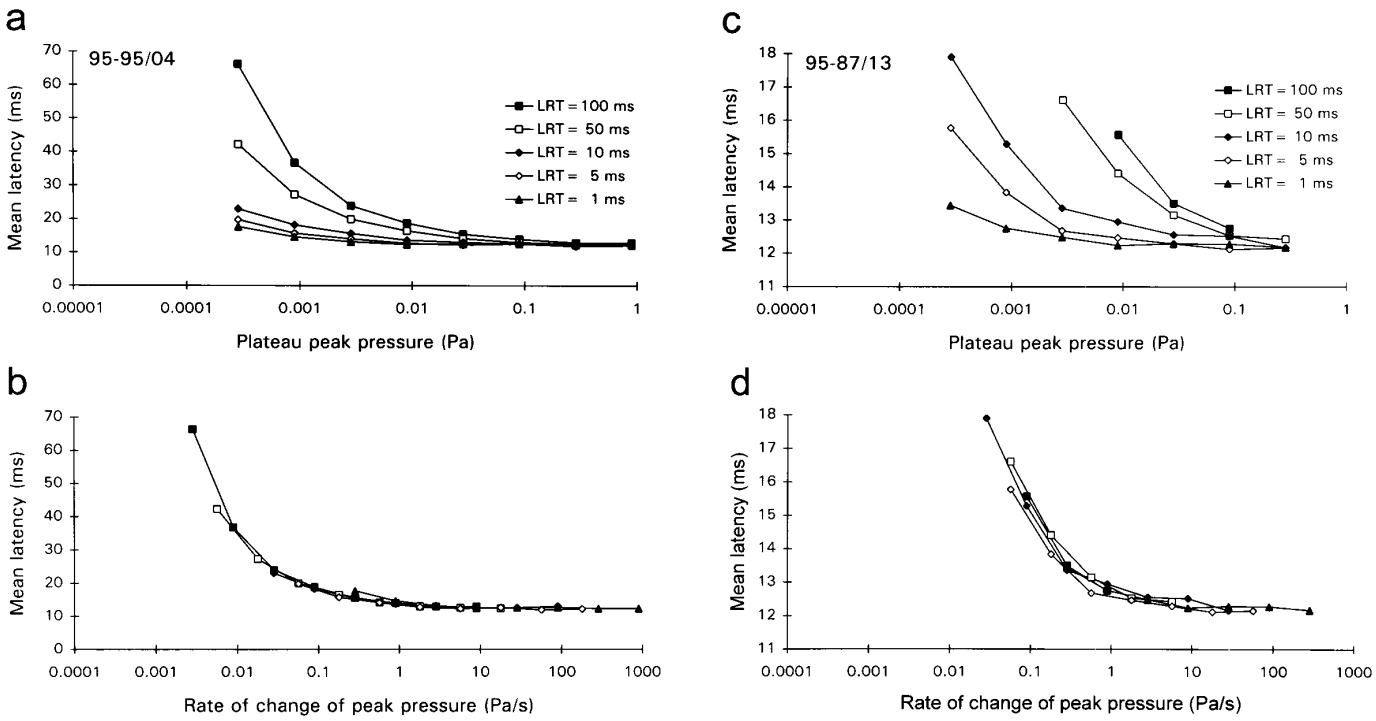

FIG. 10. Effects of rise time and plateau peak pressure of linear rise function tones on latency. Mean 1st-spike latency of *neurons 95-95/04* and *95-87/13* (*left* and *right*, respectively) to linear rise function CF tones of different plateau peak pressure and different rise time. In *a* and *c*, mean latency is plotted as a function of plateau peak pressure (in Pa). Different symbols identify different rise times (see key) and latencies to tones of the same rise time are connected. In *b* and *d*, mean latency is plotted as a function of rate of change of peak pressure. Note the close match of the latency functions obtained with the 5 different rise times.

on the responses of AI neurons (Phillips 1988). In the following, I present a post hoc analysis of latency data published in that paper, because they showed a behavior that is markedly different from that of all neurons in my sample. Figure 11, *left*, replots latency of one of the three units (viz., *RT206*) for which Phillips has presented data, and Fig. 11*a* does so in the published and conventional form, viz., as a function of plateau peak pressure or tone level (in dB SPL). As noted by Phillips (1988), for each rise time latency declines with increasing level toward asymptotic values, but the functions do not converge on a single minimum.

In Fig. 11*b*, some of these same data are replotted as functions of rise time for tones of specified plateau peak pressure. Note that for every plateau peak pressure, latency increases roughly linearly with rise time. The slopes (as well as the *Y*-intercepts) decline systematically with increasing level, but unlike those of the neurons in our sample (see Heil and Irvine 1996b), all slopes are ≥ 1 (for comparison, unity slope is illustrated by the dashed line in Fig. 11*b*). Linear regression analysis revealed slopes of 2.94 ± 0.05, 1.91 ± 0.02, 1.54 ± 0.04, 1.46 ± 0.05, and 1.05 ± 0.03 for plateau peak pressures equivalent to 22, 34, 46, 58, and 70 dB SPL, respectively. In other words, the differences in response latencies to tone bursts of the same plateau peak pressure are larger than the differences in rise time. In Fig. 11*c*, the latency data of Fig. 11*a* are plotted against the rate of change of peak pressure during the rise time. Note that the functions obtained with different rise times are not in register, quite unlike the behavior of all neurons in our sample (cf. Fig. 10, *b* and *d*). Instead, latency for tones of the same rate of change of peak pressure still increases systematically with rise time. This is more clearly illustrated in Fig. 11*d*, where latency is plotted as a function of rise time, and where each function represents latencies obtained from tone bursts characterized by the same rate of change of peak pressure.

Several points are noteworthy here. First, for any given rate of change of peak pressure latency increases with rise time, and thus increases with the plateau peak pressure of the tone bursts (cf. Fig. 9, *bottom left*), a result that at first glance may seem paradoxical or at least counterintuitive. Second, all functions can be approximated by linear functions, but their slopes do not vary with rate of change of peak pressure. In fact, the slopes relating latency to rise time were 1.01 ± 0.20, 1.06 ± 0.14, 1.03 ± 0.13, 1.02 ± 0.02, and 0.95 ± 0.06 for the five rates of change of peak pressure in ascending order, i.e., they are very close to, and not significantly different from, 1.

The only reasonable interpretation of this result is that the spikes are in fact triggered at or by the end of the rise time. This point in time is characterized by the quasi-instantaneous deceleration of peak pressure. Figure 11e therefore plots the response latency corrected for the rise time as a function of the rate of change of peak pressure. Now the five functions are in close register, and the corrected latency decreases nonlinearly with this parameter. The same results were obtained for the other two neurons for which Phillips (1988) has published latency data, and are illustrated for *RT209* in Fig. 11, *f–j*.

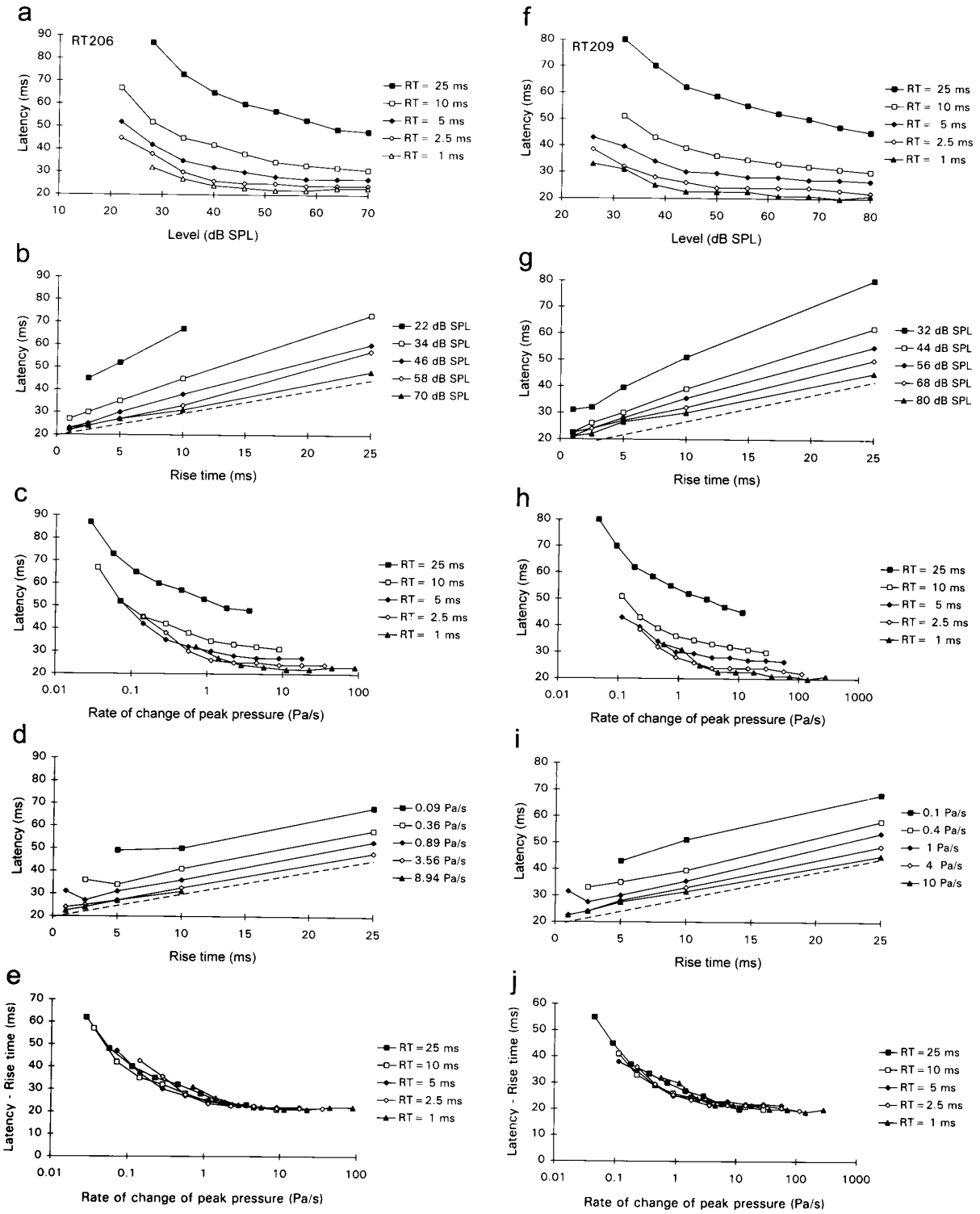

FIG. 11. Analysis of data presented by Phillips (1988) on effects of rise time and plateau peak pressure of linear rise function tones on latency of 2 neurons from cat auditory cortex (*RT206, left,* and *RT209, right*). *a* and *f* were taken from this study, and show latency to CF tones with different linear rise times (see key) as a function of SPL. In *b* and *g,* latency is plotted as a function of rise time for tones of the same plateau peak pressure (in dB SPL, see key). Note that all functions have slopes >1. Dashed lines have unity slope. In *c* and *h,* latency is plotted as a function of the rate of change of peak pressure for tones of the same rise time. Note that the functions are not in register, unlike those of the units illustrated in Fig. 10. In *d* and *i,* latency is plotted as a function of rise time for tones of the same rate of change of peak pressure. Note that latency increases directly with rise time, and thus increases with plateau peak pressure. Dashed lines have unity slope. In *e* and *j,* the rise time was subtracted from the response latency and values were plotted as a function of rate of change of peak pressure. These corrected latency functions are in close register, suggesting that in these units spikes were triggered by the quasi-instantaneous deceleration at the end of the rise time. See text for further discussion.

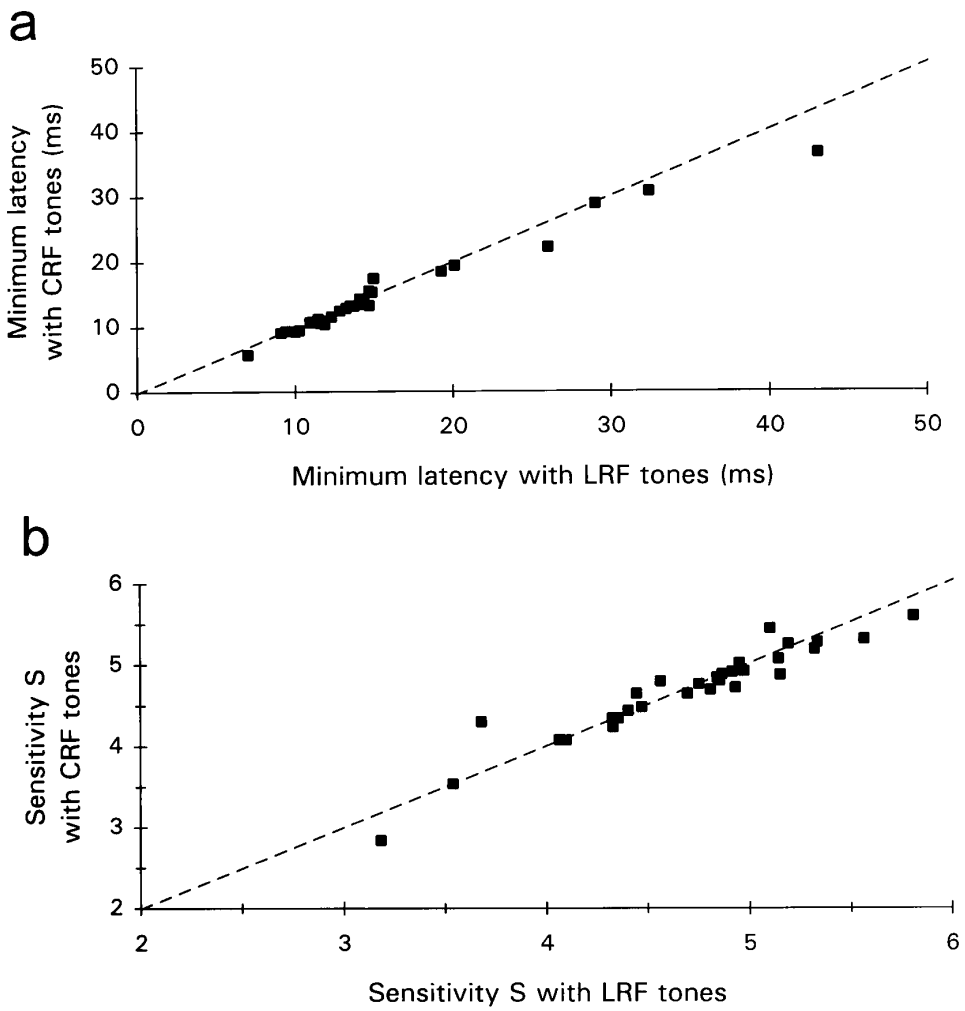

FIG. 12. Comparison of estimates derived from latency to linear and to cosine-squared rise function tones. *a*: scatterplot of minimum latencies. *b*: scatterplot of *S*. Note that both types of stimuli yield nearly identical estimates of minimum latency and of transient sensitivity. Dashed lines have unity slope.

COMPARISON OF LATENCY–RATE OF CHANGE OF PEAK PRESSURE FUNCTIONS AMONG DIFFERENT NEURONS. As was the case for latency-acceleration functions obtained with cosine-squared rise function tones, the latency–rate of change of peak pressure functions of different neurons obtained with linear rise functions tones could be brought into very close register by allowing shifts along the ordinate and the abscissa (not shown). The common form of these latency–rate of change of peak pressure functions, which differed from that of the latency-acceleration functions, and the shifts along the coordinates were found with fitting procedures analogous to those described above for cosine-squared rise functions and using the same type of formula

$$L_{LRF} = L_{min} + A_{LRF} * (\log RCPP + S)^{-4} \quad (12)$$

The weighted average of the scaling factor $\tilde{A}_{LRF}$ found with the 39 neurons studied with linear rise function tones was 1,277 ms.

COMPARISON OF LATENCY WITH LINEAR AND WITH COSINE-SQUARED RISE FUNCTION TONES. Thirty neurons were studied with both linear and cosine-squared rise function tones of the same frequency and can therefore be used for a direct comparison of the relevant features of latency functions. Figure 12*a* shows a scatterplot of the estimated minimum latencies obtained with linear and with cosine-squared rise functions tones. As expected, the two estimates are nearly identical. Note that they lie close to the line of unity slope. A linear regression analysis yielded a slope of 0.87 with $r^2 = 0.973$. Exclusion of only the rightmost point increases the slope to 0.94.

Figure 12*b* shows a scatterplot of the corresponding estimated *S* values obtained from the fits. Again, the estimates are nearly identical. A linear regression analysis yielded a slope of 0.91 with $r^2 = 0.898$.

Because the estimates of minimum latency and transient sensitivity are basically independent of the rise function, it is easy to derive the characteristics of linear and of cosine-squared rise function tones that would ideally yield a response from a given neuron with the same first-spike latency. With the formulas used here to describe the neuronal latency functions (*Eq. 8* and *12*), this is the case when

$$L_{min} + \tilde{A}_{CRF} * (\log APP_{max} + S)^{-4} = L_{min} + \tilde{A}_{LRF} * (\log RCPP + S)^{-4}$$

Rearranging terms yields

$$(\log APP_{max} + S)^4 / (\log RCPP + S)^4 = \tilde{A}_{CRF} / \tilde{A}_{LRF}$$

and

$$\log APP_{max} = (\tilde{A}_{CRF} / \tilde{A}_{LRF})^{1/4} * \log RCPP + S * [(\tilde{A}_{CRF} / \tilde{A}_{LRF})^{1/4} * - 1]$$

With $\tilde{A}_{CRF} = 12{,}791$ ms and $\tilde{A}_{LRF} = 1{,}277$ ms, it follows

$$\log APP_{max} = 1.78 * \log RCPP + 0.78S \quad (13)$$

Thus, for a given neuron and for tones of the same frequency, the isolatency conditions are described by a linear relationship between the logarithm of the rate of change of peak pressure of linear rise function tones and the logarithm of the maximum acceleration of peak pressure of cosine-squared rise function tones. The ordinate intercept is proportional to the neuron's *S*. In other words, to yield the same latency from a neuron as a cosine-squared rise function tone with a given acceleration of peak pressure, a linear rise function tone with only a low rate of change of peak pressure is required when the neuron's transient sensitivity is high, whereas a higher rate of change of peak pressure is required when the neuron's transient sensitivity is low.

SD of first-spike timing

The data presented so far have been based on the mean first-spike latency derived from up to 20 individual measures of latency on consecutive stimulus repetitions. However, the timing of the first spike varied from trial to trial. In accordance with previous studies (e.g., Aitkin et al. 1970; Brugge et al. 1969; Kitzes et al. 1978; Phillips and Hall 1990; Phillips et al. 1989), the SD of the first-spike latency around the mean will be used here as a measure of this variability.

COSINE-SQUARED RISE FUNCTIONS. The finding that with cosine-squared rise function tones a neuron's mean first-spike latency is a function of the maximum acceleration of peak pressure suggests the possibility that the SD of the first-spike latency may also be a function of this parameter.

Figures 13 and 14 present data on SD and its relationship with maximum acceleration of peak pressure for three neurons. Figures 13, *a* and *d*, and 14*a* show the now familiar finding that mean first-spike latency is a unique function of maximum acceleration of peak pressure. Figures 13, *b* and *e*, and 14*b* show the corresponding SDs of first-spike latency, also plotted against this parameter. Several observations are important.

First, SD is also inversely related to maximum acceleration of peak pressure, and consequently increases with mean latency (Figs. 13, *c* and *f*, and 14*c*).

Second, the SD of first-spike latency is also an unambiguous function of maximum acceleration of peak pressure, irrespective of the rise time or of the plateau peak pressure, and also approaches some asymptotic value. SD is more variable than mean latency when the two parameters are compared for stimuli of identical maximum acceleration of peak pressure. Therefore SD-acceleration functions were generally noisier than the mean latency-acceleration functions. As illustrated in Fig. 14*b*, the near-threshold effect, described above for mean latency, could be quite pronounced for SD.

Third, the shapes of the SD-acceleration functions are distinctly different from the shapes of the mean latency-acceleration functions. In particular, the decline in SD with acceleration is relatively steeper than the decline of mean latency for low magnitudes and relatively shallower for high magnitudes of maximum acceleration of peak pressure.

Such differences in function shape are inconsistent with a linear relationship between SD and mean first-spike latency as proposed by Phillips and Hall (1990). Instead, the shape differences suggest that SD may be proportional to the slope of the latency-acceleration function. Such a relationship would result from jitter in the effective acceleration of peak pressure, viz., in the term $(APP_{max} + S)$.

Let us therefore assume that

$$SD_{CRF} = SD_{min} + c_{CRF} * dL_{CRF}/d(\log APP_{max} + S) \qquad (14)$$

where SD_{CRF} is the SD of the first-spike latency as a function of APP_{max} and c_{CRF} is the proportionality coefficient. SD_{min} is a minimum or asymptotic SD that is independent of APP_{max}, as is the estimated minimum latency in *Eq. 8*, and would include the total jitter in those components thought to add up to the minimum latency, such as cochlear travel time, propagation of action potentials, and some synaptic factors. The term $dL_{CRF}/d(\log APP_{max} + S)$ identifies the slope of the function relating mean first-spike latency to maximum acceleration of peak pressure. This relationship can be described as in *Eq. 8*

$$L_{CRF} = L_{min} + \tilde{A}_{CRF} * (\log APP_{max} + S)^{-4} \qquad (8)$$

so that SD_{CRF} should be related to APP_{max} by

$$SD_{CRF} = SD_{min} - 4\tilde{A}_{CRF} * c_{CRF} * (\log APP_{max} + S)^{-5} \qquad (15)$$

and to the mean first-spike latency L_{CRF} by

$$SD_{CRF} = SD_{min} - 4c_{CRF} * (1/\tilde{A}_{CRF})^{1/4} * (L_{CRF} - L_{min})^{5/4} \qquad (16)$$

Thus, if the SD of the first spike were proportional to the slope of the function relating mean first-spike latency to the logarithm of the maximum acceleration of peak pressure, then the SD should grow in a nonlinear, exponential fashion with mean latency (*Eq. 16*).

This prediction was tested as follows. For each set of data, best fits to the SD-acceleration functions and to the SD–mean latency plots were found by applying *Eq. 15* and *16*, respectively. SD_{min} and c_{CRF} were allowed to vary, whereas S and L_{min} were adopted from the best solution of *Eq. 8* found for the same data set, as reported above.

The best solutions obtained for the variation of the SD of first-spike latency with maximum acceleration of peak pressure are plotted in Figs. 13, *b* and *d*, and 14*b* by solid lines without symbols. The fact that these lines are difficult to discern in the graphs actually emphasizes the high quality of the fits to the data. For the fit of the data of *neuron 95-98/14*, shown in Fig. 14*b*, the seven near-threshold points were discarded. This was the only neuron in which the inclusion of the near-threshold points severely impaired the quality of the fit.

The exponential functions describing the relationship between SD and mean latency (*Eq. 16*), which emerged from the same fitting procedure, are also plotted by solid lines in Figs. 13, *c* and *f*, and 14*c*. Note their good approximation of the data.

For comparison, the dashed lines in these charts represent the best linear fits to the data. In some cases linear fits would systematically underestimate the SDs at short mean latencies and systematically overestimate them at longer mean latencies (e.g., *neuron 95-98/11*, Fig. 13*c*). Nevertheless, and in agreement with previous findings (Phillips and Hall 1990), linear fits did provide good descriptions of the relationships between SD and mean latency: values of r^2 were as high as 0.969 with a weighted average of 0.610. However, the nonlinear fits proposed here (*Eq. 16*) were in some cases

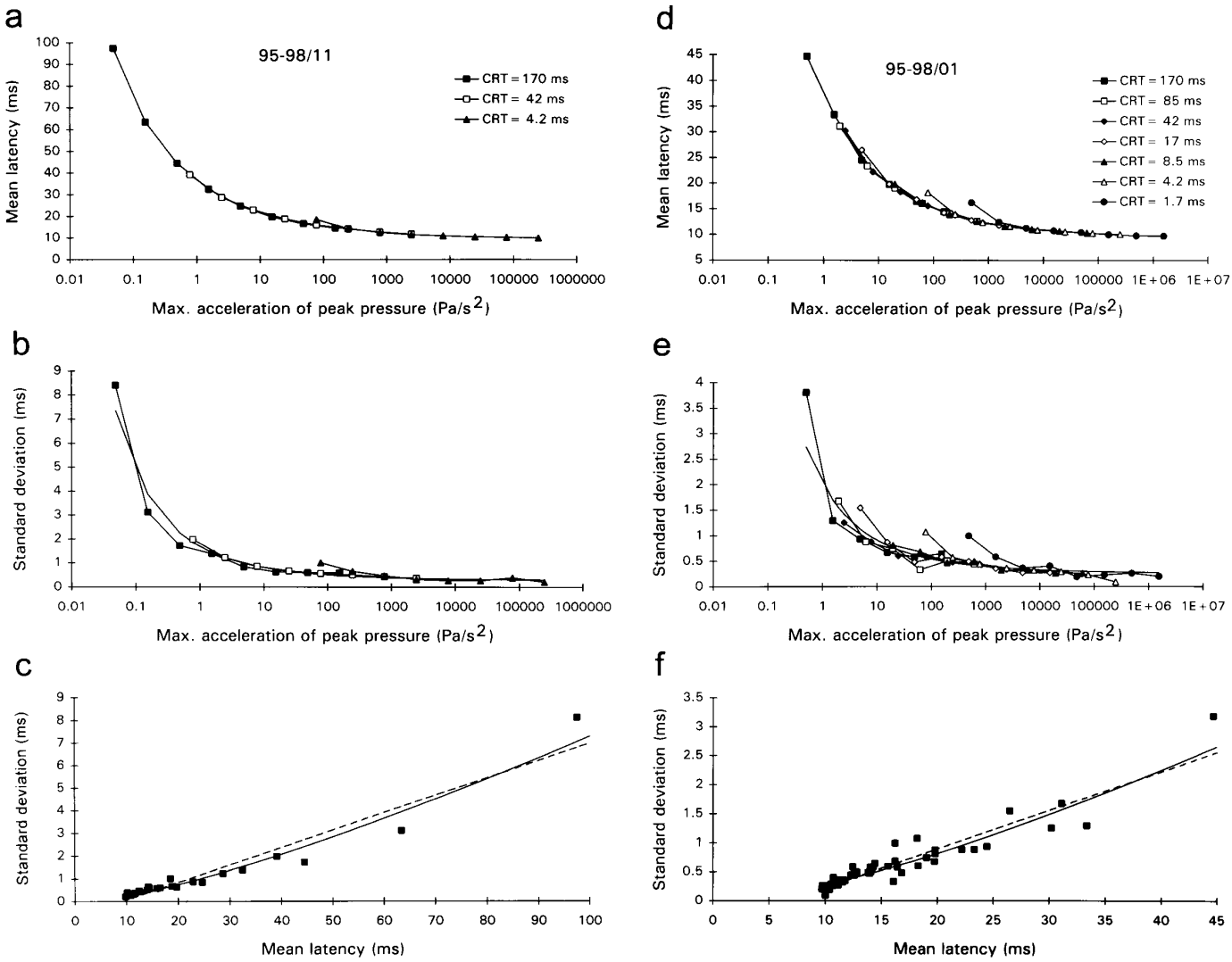

FIG. 13. Comparison of SD and mean of 1st-spike latency. Data from *neuron 95-98/11* (*a*–*c*), stimulated with contralateral CF tones of 10.3 kHz, and from *neuron 95-98/01* (*d*–*f*), stimulated binaurally with CF tones of 20.3 kHz, are illustrated. *a* and *c*: mean 1st-spike latencies obtained with tones of different cosine-squared rise times (see keys) plotted against maximum acceleration of peak pressure. *b* and *e*: corresponding SDs of 1st-spike latency also plotted against maximum acceleration of peak pressure. Note that the functions obtained with different rise times are in close register. Solid lines without symbols: best fits of *Eq. 15* to the data sets. The equation assumes that the SD is proportional to the slope of the mean latency-acceleration function. *c* and *f*: scatterplots of the SD of 1st-spike latency against the mean. Solid lines: best fits of *Eq. 16* to the data sets. Dashed lines: best linear fits. See RESULTS for further explanations.

markedly better than linear fits (up to 40%). Averaged over the entire data sample, the nonlinear functions provided a fit that was ~2% better than the linear functions. In a small number of data sets, SD appeared to be independent of maximum acceleration of peak pressure, and thus also independent of mean first-spike latency. This was the case with 10 linear and 8 nonlinear fits. These data sets were all among those with the smallest numbers of first spikes.

Figures 15 and 16 show the population data for the proportionality coefficient and the estimated minimum SD. In Fig. 15, the c_{CRF} of *Eq. 15* and *16* is plotted against the number of first spikes that contributed to the fit. This coefficient shows a unimodal distribution, which narrows rapidly with increasing number of first spikes and converges on the weighted average of $c_{CRF} = -0.102$. This observation is reminiscent of the one made above for the scaling factor A (Fig. 4*a*), used in the description of the latency–acceleration functions. Thus c_{CRF} between SD and slope of the latency-acceleration function may in fact be very similar across the neuronal pool and the range of stimulus conditions used here. For a description of the average relationship between SD and acceleration of peak pressure, *Eq. 15* may therefore be written as

$$SD_{CRF} = SD_{min} + 5.2 * 10^3 * (\log APP_{max} + S)^{-5} \quad (17)$$

and *Eq. 16* as

$$SD_{CRF} = SD_{min} + 0.04 * (L_{CRF} - L_{min})^{5/4} \quad (18)$$

Figure 16 provides a scatterplot of the estimated SD_{min} against the estimated L_{min}. SD_{min} increases continuously with L_{min}, but note that the distribution of the points does not suggest a linear but rather a power relationship between the

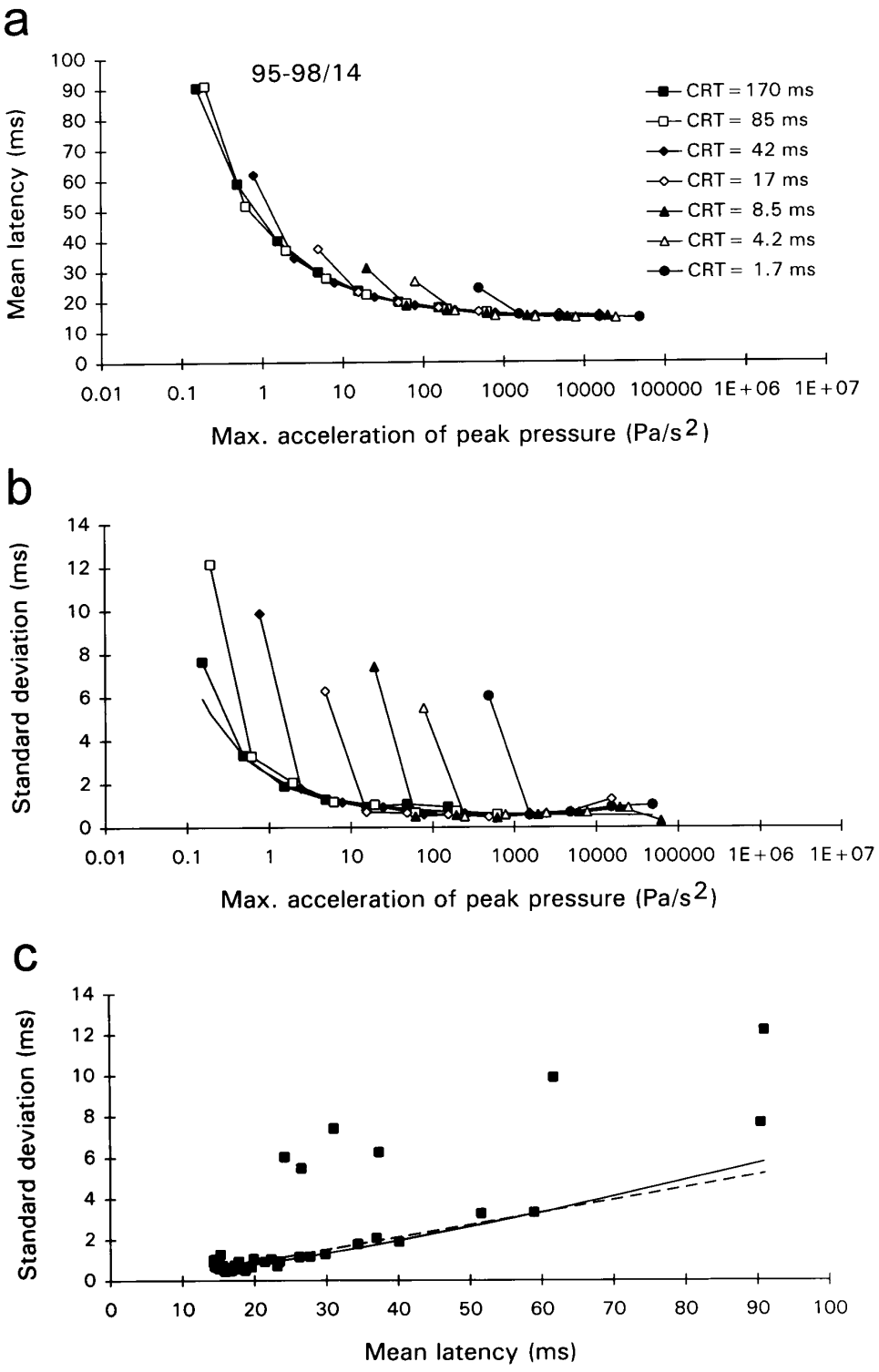

FIG. 14. Comparison of SD and of mean of 1st-spike latency. Data are from *neuron 95-98/14*, stimulated binaurally with CF tones of 5.5 kHz. Note the pronounced near-threshold effects for both mean and SD of 1st-spike latency. The 7 near-threshold points were discarded for the fits of the functions relating SD to maximum acceleration of peak pressure and to mean latency in *b* and *c*, respectively. All other conventions as in Fig. 13.

two parameters. With L_{min} approaching zero, SD_{min} converges against zero (Fig. 16, – – –).

LINEAR RISE FUNCTION TONES. Comparable results were obtained with linear rise function tones. Data from one neuron (*95-92/02*) are illustrated in Fig. 17. With linear rise function tones, SD of first-spike latency is an inverse function of the rate of change of peak pressure (Fig. 17*b*), just as for mean latency (Fig. 17*a*). The systematic differences in the shapes of the functions relating mean latency and SD to rate of change of peak pressure again suggest that SD may be proportional to the slope of the function relating mean latency to rate of change of peak pressure

$$SD_{LRF} = SD_{min} + c_{LRF} * dL_{LRF}/d(\log RCPP + S) \quad (19)$$

and therefore

$$SD_{LRF} = SD_{min} - 4c_{LRF} * \hat{A}_{LRF} * (\log RCPP + S)^{-5} \quad (20)$$

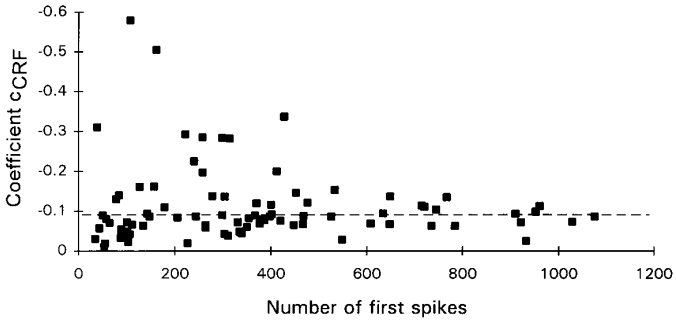

FIG. 15. Scatterplot of the proportionality coefficient c_{CRF}, relating the SD of the 1st-spike latency to the slope of the latency-acceleration function (*Eq. 15*), plotted against the number of 1st spikes having contributed to the fit. Note that with increasing number of 1st spikes the distribution rapidly converges against the weighted average of $c_{CRF} = -0.1016$ (– – –).

And the relationship with the mean latency is then given by

$$SD_{LRF} = SD_{min} - 4c_{LRF} * (1/\hat{A}_{LRF})^{1/4} * (L_{LRF} - L_{min})^{5/4} \quad (21)$$

The solid lines in Fig. 17, *b* and *c*, represent the best fits of *Eq. 20* and *21* to the data, whereas the dashed line in Fig. 17*c* represents the best linear fit. Again, although linear fits provided a good description of the relationship between SD and mean latency, *Eq. 21* provided yet a better fit, both for the neuron illustrated in Fig. 17 and, on average, for the entire data sample (not shown). The width of the distribution of the c_{LRF} also decreased with the number of first spikes that contributed to the fit (not shown), with a weighted average of $c_{LRF} = -0.119$. This number is close to the one obtained with cosine-squared rise functions signals, viz., -0.102 (see above).

On average then, *Eq. 20* can be written as

$$SD_{LRF} = SD_{min} + 0.6 * 10^3 * (\log RCPP + S)^{-5} \quad (22)$$

and *Eq. 21* as

$$SD_{LRF} = SD_{min} + 0.08 * (L_{LRF} - L_{min})^{5/4} \quad (23)$$

COMPARISON OF COSINE-SQUARED AND LINEAR RISE FUNCTION TONES. Figure 18*a* shows a scatterplot of the estimated minimum SDs obtained with linear and cosine-squared rise function tones. Both stimuli yielded very similar estimates, the points lying close to the line of unity slope. A linear regression analysis yielded a slope of 0.75 with $r^2 = 0.912$. Exclusion of only the rightmost point increased the slope to 0.98 with $r^2 = 0.938$. In Fig. 19, the estimated minimum SD obtained with linear rise function tones is plotted against the estimated minimum first-spike latency (open circles). This plot also suggests a nonlinear relationship between the two estimates. To emphasize the similarity with the results obtained with cosine-squared rise functions, the data of Fig. 16 are retained in Fig. 19 (solid squares).

Figure 18*b* provides a scatterplot of the proportionality coefficients between SD of first-spike latency and the slopes of the functions relating mean latency to rate of change and to acceleration of peak pressure, obtained with linear and with cosine-squared rise function tones, respectively. The two estimates are also correlated, although more loosely than those of minimum SD. A regression analysis yielded a slope of 1.21 ± 0.13 with $r^2 = 0.761$. Exclusion of the rightmost data point decreased the slope to 1.09 ± 0.17. The slope is not significantly different from 1 (dashed line). With one exception, all data points are below the line with a slope of 1.78 (dot-dashed line). This slope would have been expected if there were a fixed exponential relationship between SD and mean latency, irrespective of the rise function. If this were the case, the coefficients of *Eq. 18* (i.e., 0.04) and *23* (i.e., 0.08) should have been identical. Rather, comparison of these equations, which provide average descriptions of the data, reveals that for any given mean latency ($L_{LRF} = L_{CRF}$) the difference between the corresponding SD and the minimum SD is twice as high for linear as for cosine-squared rise function tones

$$(SD_{LRF} - SD_{min}) = 2 * (SD_{CRF} - SD_{min}) \quad (24)$$

Figure 20 shows, for three neurons, scatterplots of the SD against the mean first-spike latency to CF tones shaped with linear and with cosine-squared rise functions. Note that SD above the estimated minimum SD grows with mean latency at a higher rate for linear rise function tones than for cosine-squared rise function tones.

These observations, as summarized by *Eq. 24*, are also difficult to reconcile with the assumption of a linear relationship between SD and mean first-spike latency. However, they are compatible with the suggestion made here that the SD may originate from jitter in the effective acceleration (i.e., $\log APP_{max} + S$) or the effective rate of change of peak pressure (i.e., $\log RCPP + S$). It follows from *Eq. 8* and *12* that for a given neuron (same *S*) and for any two linear and cosine-squared rise function tones that yield the same mean latency, the SD produced by the same jitter in *S* (say ± 0.1) will be about twice as high for linear as for cosine-squared rise functions.

DISCUSSION

The present paper demonstrates that first-spike latency of auditory cortical neurons is an unambiguous function of acceleration of peak pressure at tone onset for cosine-squared rise function tones, and of the (constant) rate of change of peak pressure for linear rise function tones. With linear rise functions, acceleration of peak pressure is mathematically instantaneous and infinite in amplitude. However, the acoustic signal is transformed into a receptor potential, and, as jugded from intracellular recordings of inner hair cells (e.g., Russell and Sellick 1983), the rise of the DC receptor potential to high-frequency tones shaped with linear rise functions

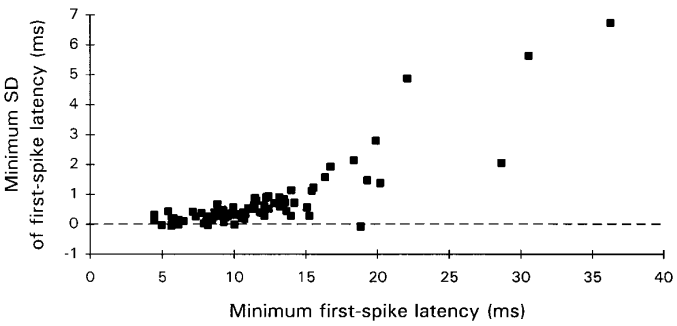

FIG. 16. Scatterplot of the estimated SD_{min} of 1st-spike latency against the estimated L_{min}. SD_{min} approaches 0 (– – –) with L_{min} approaching 0. Also note that SD_{min} grows in a distinctly nonlinear fashion with L_{min}.

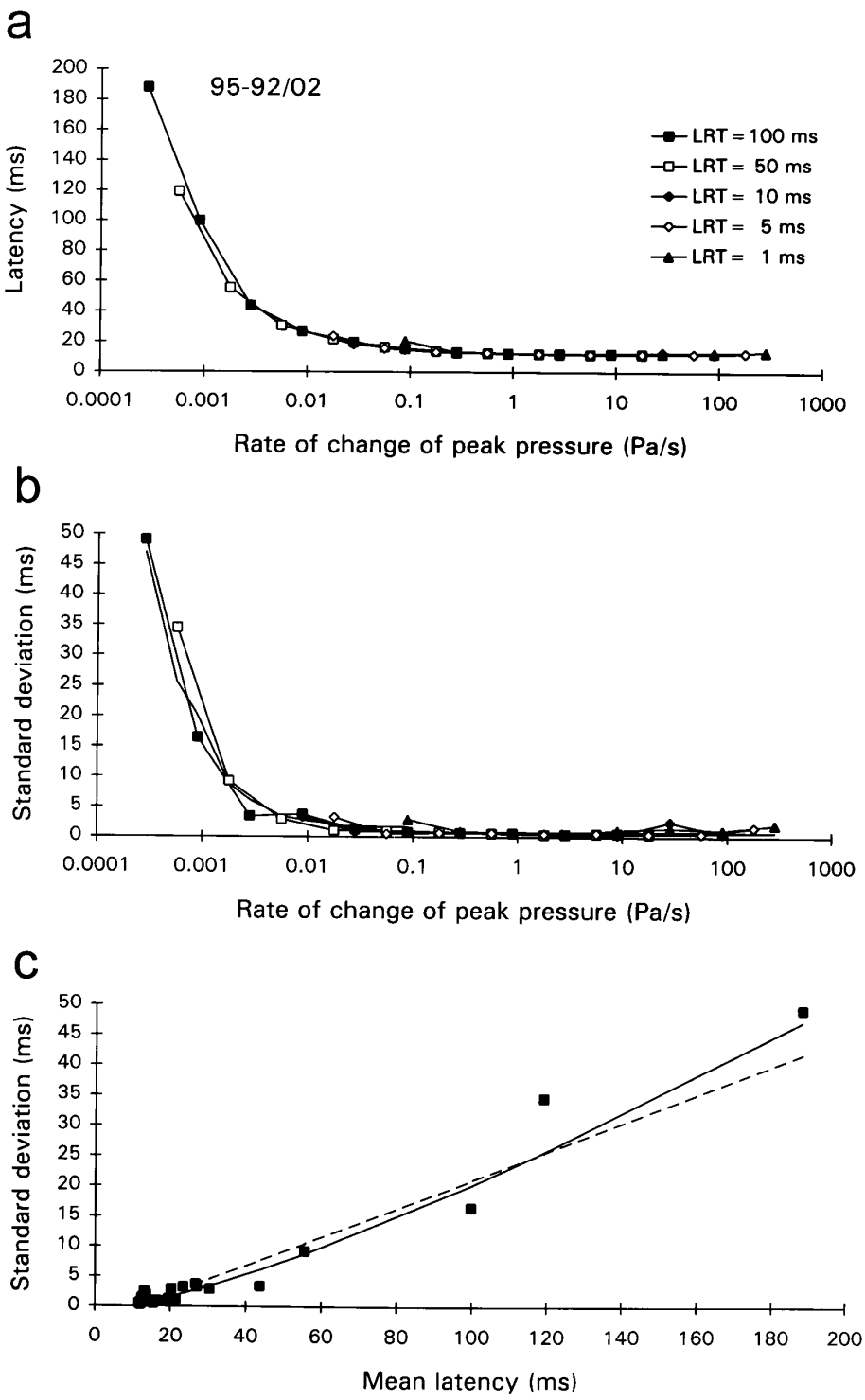

FIG. 17. Comparison of SD and of mean of 1st-spike latency obtained with linear rise function tones. Data are from *neuron 95-92/02*, stimulated with contralateral CF tones of 18.5 kHz. Other conventions as in Fig. 13.

is no longer precisely linear, but rather somewhat curvilinear. Consequently, the rate of rise of the DC receptor potential is no longer constant, and its acceleration is no longer instantaneous and infinite. Acceleration of the DC receptor potential may rather be a rapidly decaying function of time (in principle similar to the course of acceleration of peak pressure in cosine-squared rise function tones; Fig. 1). Thus, with linear rise function tones, latency may also be a function of the (transformed) acceleration at tone onset, a view also favored by the finding that latency to such tones could be determined very early during the rise time (i.e., within <1 ms). For both cosine-squared and linear rise functions, acceleration is maximal at the beginning of the rise time. The present study therefore cannot resolve the question of whether it is the magnitude of the initial or the maximum acceleration occurring during the rise time that is the critical value.

The initial time course of the peak pressure in signals

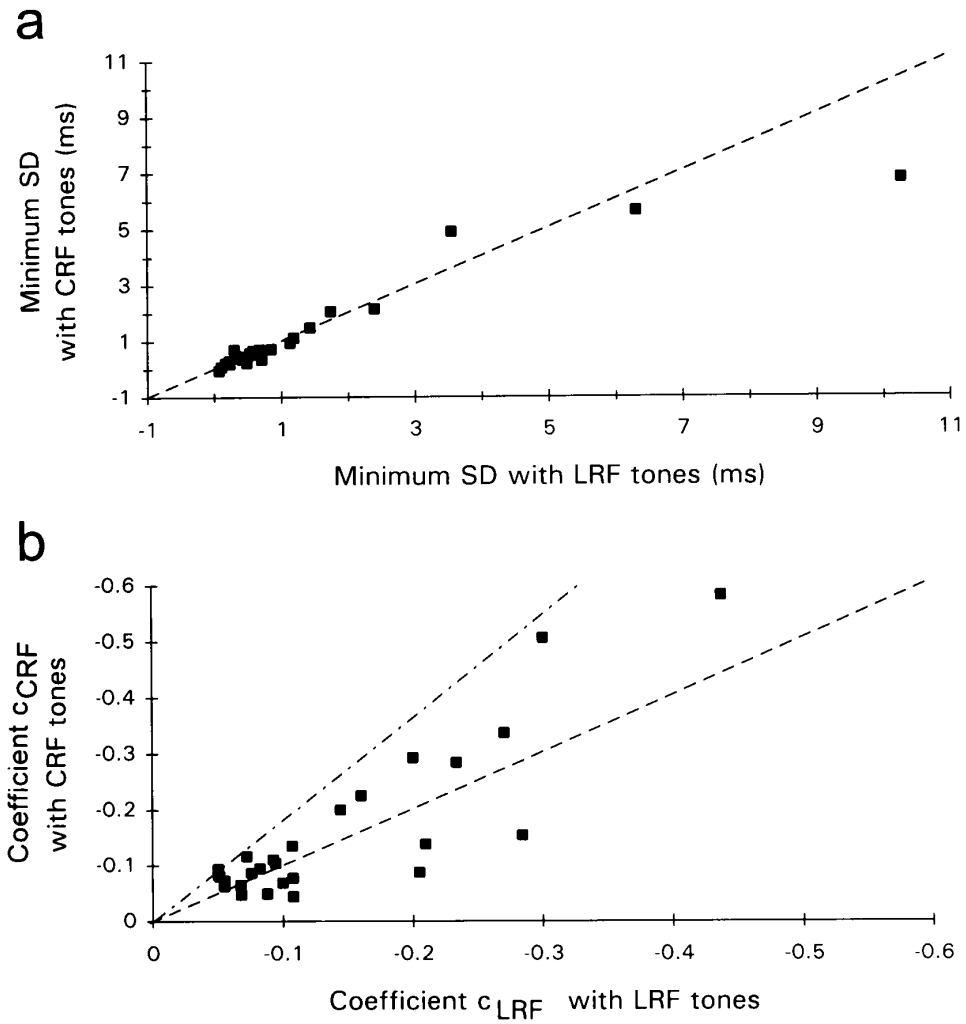

FIG. 18. Comparison of estimates derived from SD to linear and to cosine-squared rise function tones. *a*: scatterplot of the estimated minimum SDs. *b*: scatterplot of the proportionality coefficient between SD and slope of the functions relating mean latency to rate of change (c_{LRF}) and to acceleration of peak pressure (c_{CRF}), respectively. Note that both types of stimuli yield nearly identical estimates of minimum SD and similar estimates of the proportionality coefficients. Dashed lines have unity slope. Dot-dashed line in *b* has a slope of 1.78. This slope would have been expected if there were a fixed exponential relationship between SD and mean latency, irrespective of the rise function. Note that nearly all points fall well below this line. See RESULTS for further explanation.

with a common maximum acceleration or a common rate of change of peak pressure is very similar or identical (see Figs. 1 and 9, *bottom left*), so that it may be argued that such signals could reach some (very low) firing threshold peak pressure at nearly the same time and therefore lead to a response with the same latency. However, careful analysis of latency of responses to linear rise function tones of different rise time and plateau peak pressure showed that the change in a neuron's latency with alterations of rate of change of peak pressure is incompatible with such a firing threshold interpretation of latency and the opposite of what would be expected if adaptive processes were to prolong the time necessary to reach the presumed threshold for long rise times or low rates of change of peak pressure (Heil and Irvine 1996b). Furthermore, as is shown in the companion paper, the first spike can be triggered at very different signal amplitudes, even for signals that share the same acceleration or, with linear rise functions, the same rate of change of peak pressure.

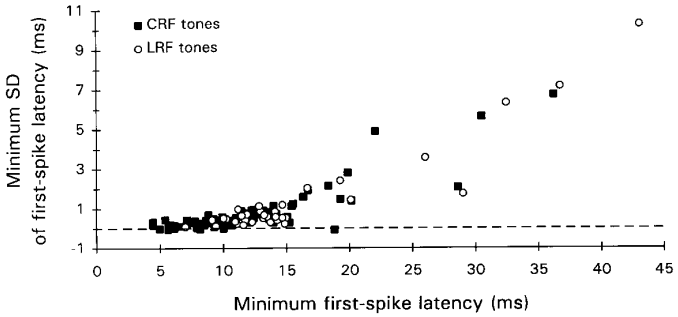

FIG. 19. Scatterplot of the estimated SD_{min} of 1st-spike latency against the estimated L_{min}. Data obtained with linear and with cosine-squared rise function tones are shown by open circles and solid squares, respectively. Other conventions as in Fig. 16.

Comparison with previous studies

Acceleration of peak pressure has previously not been recognized as a relevant parameter of acoustic signals. But this parameter has been varied, almost certainly without the experimenters' awareness, in a huge number of studies, e.g., in all those in which stimulus manipulations affected the SPL at the eardrum, whereas rise time and rise function were kept constant. In the context of the recent proposal of a temporal code for sound location by cortical neurons (Middlebrooks et al. 1994), it is worth emphasizing that the SPL is also affected by changes in a sound source's position in three-dimensional space (azimuth, elevation, and distance) given the frequency-dependent shadowing effect of the head

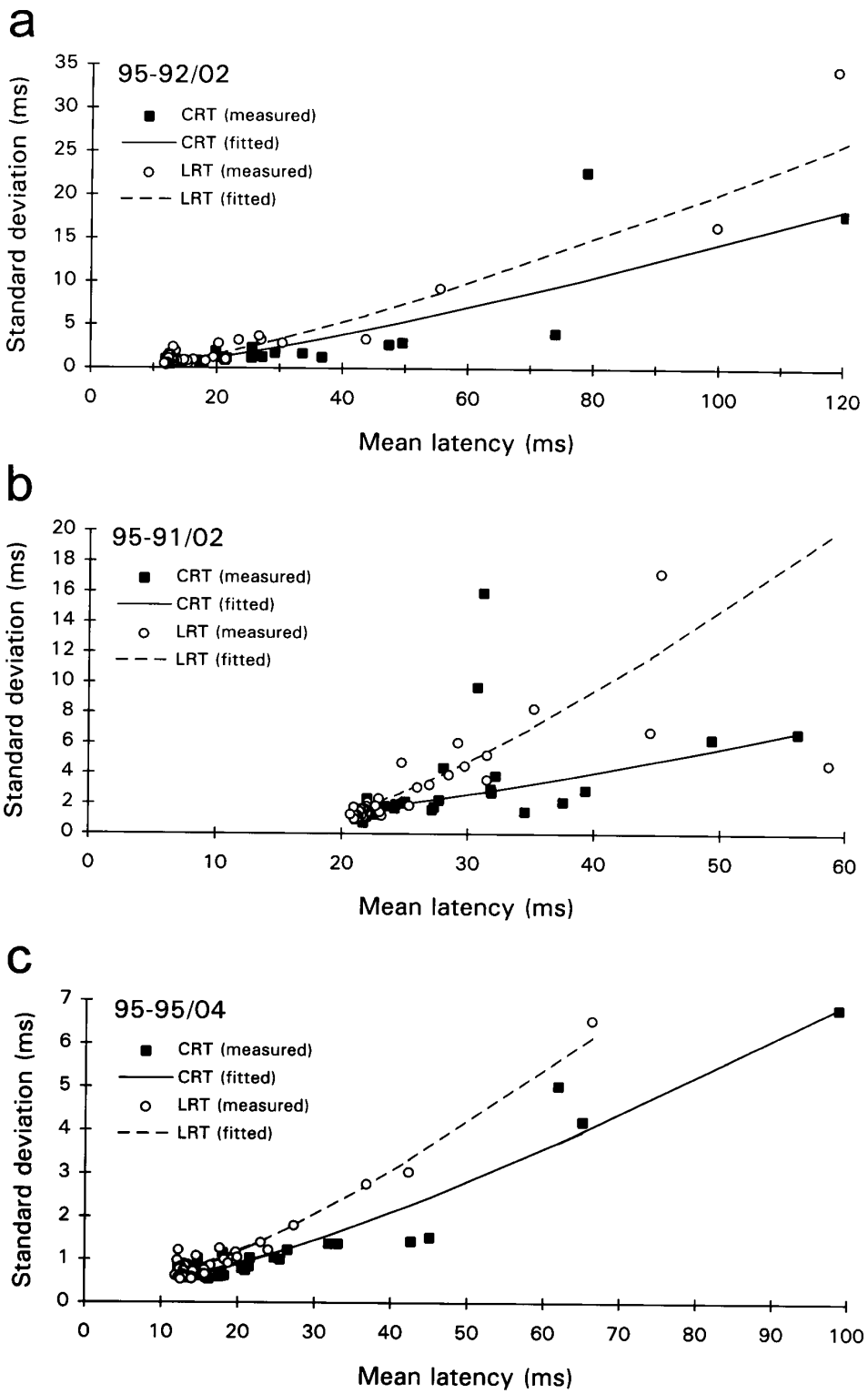

FIG. 20. Comparison of the growth of SD with mean latency for linear and for cosine-squared rise function tones. Data for 3 neurons are shown. *Neuron 95-91/02* was stimulated with binaural tones of 15.5 kHz, *neuron 95-92/02* with contralateral tones of 18.5 kHz, and *neuron 95-95/04* with contralateral tones of 22 kHz. Solid and dashed lines: best fit of *Eq. 16* and *21*, respectively. Note that SD grows with mean latency at a higher rate for linear rise function tones than for cosine-squared rise function tones.

and the frequency-dependent pressure transformations performed by the pinna (for review see Carlile 1996). The neglect of acceleration in onsets has likely been due to the focus of attention on features characteristic of the steady-state parts of signals, such as the SPL or, in binaural studies, interaural intensity differences. Thus, in previous studies, latency was usually plotted as a function of SPL, and was found to be inversely related to it (e.g., Aitkin et al. 1970; Brugge et al. 1969; Hind et al. 1963; Kitzes et al. 1978; Phillips 1985, 1988; Phillips and Hall 1990; Phillips et al. 1989). Rise functions of artificial auditory signals have mainly been introduced with the purpose of reducing spectral splatter at signal onsets. However, even in studies specifically designed to investigate the effects of the shape of tone

onsets on neuronal responses by altering rise times, neuronal response properties were plotted with respect to SPL (Phillips 1988; Phillips et al. 1995).

For all AI neurons sampled in the present study, latency was a function of the positive acceleration occurring at the beginning of the rise time. However, the post hoc analysis of data published previously by Phillips (1988) showed that for these neurons the first spike is triggered at the end of the rise time, i.e., at the instant of deceleration of peak pressure (see Fig. 11). A consequence of this behavior is that when signals are grouped according to the same rate of change of peak pressure during the rise time, latency increases with rise time, and thus increases with tone level, a phenomenon that at first glance seems paradoxical. Phillips (1988) did not measure first-spike latency, but instead latency was defined as the interval between stimulus onset and the peak bin of the poststimulus time histogram. Although this methodological difference is highly unlikely to account for the observed differences in response latency between the present data and those of Phillips, there may be further, undetected, methodological differences between the two studies. On the other hand, it cannot be excluded that there might be two classes of cells in auditory cortex, in one of which the latencies are a function of acceleration and in the other a function of deceleration of peak pressure. The latter neurons might be either very rare, or located in areas that were not surveyed in the present study, although we probably did study a representative sample of AI neurons, as judged by their distributions of CF and minimum latency, their frequency tuning and binaural characteristics (see *Data base*), and the shapes of their spike count functions (see companion paper).

SD of first-spike latency was shown here also to be a function of maximum acceleration or, for linear rise function tones, of rate of change of peak pressure. In previous studies, SD was plotted as a function of tone level (e.g., Aitkin et al. 1970; Brugge et al. 1969; Kitzes et al. 1978; Phillips 1985, 1988; Phillips and Hall 1990; Phillips et al. 1989), and in two studies as a function of mean first-spike latency (e.g., Phillips and Hall 1990; Phillips et al. 1989). Although Phillips and Hall proposed a linear relationship between SD and mean latency, several observations in the present study are incompatible with a linear relationship. The different growth rates of SD with mean latency for cosine-squared and linear rise function tones (Fig. 20) and the finding that SD declined more rapidly than latency with acceleration (or rate of change) of peak pressure for low values of this parameter and less rapidly for higher values are difficult to reconcile with a linear relationship. Careful inspection of previous publications (e.g., Aitkin et al. 1970; Brugge et al. 1969; Kitzes et al. 1978; Phillips and Hall 1990) reveals that the latter result was also obtained by these authors. The nature of the differences in the shapes of the functions relating mean latency and SD to maximum acceleration (or rate of change) of peak pressure suggested that SD is proportional to the slope of the functions relating mean latency to acceleration (or rate of change) of peak pressure, and this relationship described the data somewhat better than a linear one. Jitter in the effective acceleration of peak pressure, i.e., in the term ($\log APP_{max} + S$) of *Eq. 8* or, for linear rise function tones, jitter in the effective rate of change of peak pressure, i.e., in the term ($\log RCPP + S$) of *Eq. 12*, would cause or closely approach such a relationship. Thus jitter in the neuronal S or jitter in the way in which a given acceleration or rate of change of peak pressure is represented in the motion of the basilar membrane, i.e., jitter in peripheral mechanics and cochlear amplifiers, might underlie the SD of first-spike timing. The finding that the proportionality coefficient between SD and the slope of the latency functions is so similar across the neuronal population, and similar for the two rise functions, also favors this notion.

I have also assumed a minimum SD, thought to reflect the jitter in the same processes that underlie the minimum latency, such as cochlear travel time, axonal travel times, and synaptic factors. Whereas these delays simply add up to yield a minimum latency, this will not be the case for the minimum SD. For example, at every synapse along the pathway the variability of first-spike timing in the afferent axon(s) would be expected to increase (or decrease, see, e.g., Joris et al. 1994) by some factor in the postsynaptic neuron. Thus a nonlinear relationship between minimum SD and minimum latency should be expected, in line with the finding of the nonlinear growth of the minimum SD with the minimum mean latency (Figs. 16 and 19).

Other factors influencing first-spike latency

Although first-spike latency is a function of the acceleration/rate of change of peak pressure at tone onset, this is not to say that a particular acceleration/rate of change in a signal will under all circumstances evoke a response from a neuron with the same latency. The near-threshold effect, as described in this paper (e.g., Fig. 14), is a case in point. The laterality of stimulus presentation is another factor. Laterality does not appear to influence the shape of latency–acceleration/rate of change functions, but it affects the functions' position along the ordinate, i.e., it affects the minimum latency. In the few neurons excited by stimulation of either ear, studied here, minimum latency was systematically longer by 2–3 ms for ipsilateral stimulation than for contralateral or binaural stimulation. This could reflect one or two additional synapses, slower conduction velocities, or longer lengths of the ipsilateral pathways to these neurons.

Latency of a given neuron is also a function of frequency, generally being shortest at or near the CF for tones of the same plateau peak pressure and rise time (e.g., Aitkin et al. 1970; Brugge et al. 1969; Heil et al. 1992a; Hind et al. 1963; Kitzes et al. 1978). The present study shows in addition that the forms of the functions relating latency to acceleration are very similar for different frequencies, and that it is their position along the acceleration axis that differs systematically with frequency. Latency to a tone burst has also been shown to increase by up to 3 ms when the tone burst is preceded by a masking tone (Calford and Semple 1995). Similarly, latency also increases with the repetition rate of tone bursts (Phillips and Hall 1990; Phillips et al. 1989), a parameter that was not varied in the present study. Close inspection of the figures provided by Phillips and coworkers (Figs. 1*c*, 2*c*, and 8*b* in Phillips et al. 1989; Fig. 3*a* in Phillips and Hall 1990) reveals that the effect of repetition rate on latency seems to be a systematic displacement of the latency functions (i.e., latency-level functions) along the

ordinate. This suggests that the effects of repetition rate and frequency on latency are different in origin. And finally, latency to tone bursts is prolonged when the tone bursts are presented after the onset of a long-duration broadband noise masker (Phillips 1985). Inspection of the relevant figures (Figs. 2, *c* and *f*, 6, and 7, *c* and *f*) suggests that background noise has a similar effect as frequency, i.e., brings about a displacement of the latency functions along the abscissa.

Common shape of latency-acceleration functions

A comparison of latency-acceleration functions, or of latency–rate of change of peak pressure functions, among different neurons or stimulus conditions revealed that they are all of strikingly similar shape despite differences in the position and in the extent of these functions along the coordinates. The latter observation simply reflects differences in the shape of the spike count functions (see companion paper for a detailed account of these issues).

The mathematical function selected to describe the similar shape of the latency-acceleration (or rate of change of peak pressure) functions and to quantify their different positions in the coordinate system (*Eq. 8* and *12*) may not adequately reflect the (unknown) nature of the physical and biochemical processes that may underlie the generation of the latency–acceleration/rate of change of peak pressure relationships. However, it provides an excellent approximation of the functions, it is simple, it quantifies the dispersion of the functions along either coordinate, and it makes the reasonable assumption that the latency of a neuron contains components that are independent of the magnitude of the stimulus. These components, such as acoustic delays, cochlear travel time (e.g., Robles et al. 1976; Ruggero and Rich 1987), axonal travel times, and possibly some synaptic components, simply add up and yield a minimum latency.

The estimated minimum latencies varied considerably for different neurons (Fig. 7), a finding readily expected in light of the diversity of pathways over which they may derive their inputs, even at CF. Furthermore, the shortest estimated minimum latencies decreased with increasing CF. Such a trend would have to be expected if cochlear travel time is one of the components contributing to the estimated minimum latency. A similar decrease in latency to CF tones with increasing CF was also observed in other nuclei of the auditory pathway (e.g., Heil and Scheich 1991; Heil et al. 1995; Kitzes et al. 1978; Langner et al. 1987), although latency was measured either at some fixed tone level or at some level above firing threshold (30–60 dB in different studies).

The differences in the horizontal positions of the latency–acceleration/rate of change of peak pressure functions reflect differences in sensitivity to acceleration or rate of change of peak pressure (transient sensitivity). It is worth reemphasizing here that this measure is not equivalent to the firing threshold of the neuron (Fig. 5), although for a given neuron the transient sensitivity-frequency filter functions and the conventional tuning curves share some characteristics (Fig. 6). Neurons with the same transient sensitivity, reflected in a common position of their latency–acceleration/rate of change of peak pressure functions along the abscissa, can differ in firing threshold by some 100 dB (Fig. 5). Moreover, in response to tones of the same frequency, the measure of transient sensitivity is unambiguous, i.e., it is a single value, whereas firing threshold in dB SPL can increase with rise time (see Fig. 6, *b* and *e*) (Phillips 1988; but see companion paper). The distribution of transient sensitivities at CF for different neurons is also a function of frequency, and appears to be grossly similar to the cat's audiogram. For comparison, the reader is referred to a study by Rajan et al. (1991) that summarizes a range of N_1 audiograms measured under various experimental conditions in barbiturate-anesthetized cats. Although N_1 thresholds depend critically on stimulus paradigms, such as rise time, and other conditions, audiogram shapes are fairly similar, particularly for frequencies >3 kHz.

Possible origin of the latency–acceleration/rate of change of peak pressure relationship

The finding of nearly identical shapes of latency–acceleration/rate of change of peak pressure functions among different neurons and different stimulus conditions is surprising given the enormous degree of convergence and divergence of connections at nuclei peripheral to the cortex, as well as within the cortex itself, and given that cortical cells are likely to differ widely in the number of serial synapses in their afferent pathways. However, the findings that the shortest estimated minimum latencies decrease with increasing CF, that the distribution of estimated transient sensitivities grossly parallels the cat's audiogram, and that the relationship between SD and first-spike latency could possibly be accounted for by jitter in peripheral mechanics, suggest that the common relationship between latency and acceleration/rate of change of peak pressure may have its origin in the peripheral auditory system. The latencies of basilar membrane vibration and of the receptor potential of inner hair cells appear to be independent of the amplitude of acoustic stimuli, such as clicks (Robles et al. 1976), whereas in response to similar stimuli the latencies of auditory nerve fibers are a sensitive function of amplitude (e.g., Pfeiffer and Kim 1972). If these findings can be extrapolated to stimuli with longer rise times, it then appears that the relationship between latency and acceleration/rate of change of peak pressure originates in the synapses between inner hair cells and afferent fibers. This proposal requires that the same relationship between latency and acceleration as seen in cortical cells must exist in the auditory nerve.

Functional implications

Although a particular acceleration or rate of change of peak pressure at tone onset is transformed into a particular neuronal latency in a smooth analog fashion, the brain has no means of measuring the latency. However, one way for the brain to derive useful information through latency is by means of a comparison of the timing of spikes across a neuronal population, as originally proposed by Hind et al. (1963). It has long been recognized, for example, that differences in the timing of inputs from the two ears provide an important cue for sound localization, and that the differences are extracted via appropriate delays and coincidence detection mechanisms in brain stem auditory nuclei (e.g., Goldberg and Brown 1969; Overholt et al. 1992; Yin and Chan

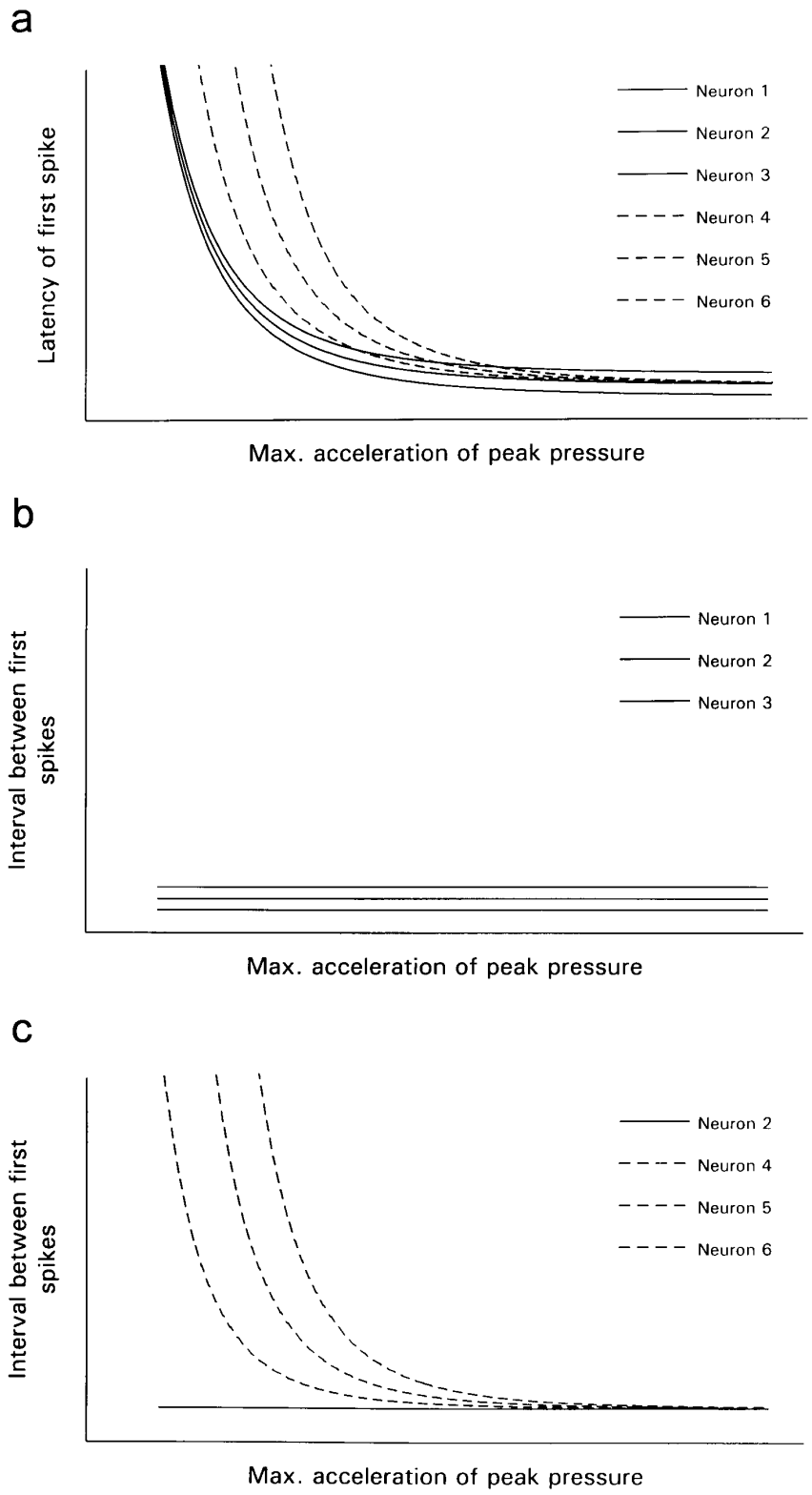

FIG. 21. Schematic latency-acceleration functions of 6 hypothetical auditory neurons. *Neurons 1–3* have identical transient sensitivity, but differ in minimum latency. *Neurons 4–6* have identical minimum latency (the same as *neuron 2*), but differ in transient sensitivity, both from each other and from *neurons 1–3*. Note that the relative timing of the 1st spikes is independent of the magnitude of the acceleration of peak pressure for neurons with the same transient sensitivity, i.e., *neurons 1–3* (*middle*), whereas the 1st spikes disperse with decreasing acceleration for neurons with the same minimum latency but with different transient sensitivity, i.e., *neurons 2* and *4–6* (*bottom*).

1990). Likewise, interaural intensity differences of otherwise identical signals will lead to interaural latency differences from the two ears, and thus interaural intensity differences could be processed in a similar way as neural time differences (''latency hypothesis''; Jeffress 1948). However, as suggested by the present study, such latency differences would not be brought about by the intensity differences per se, but rather by the associated differences in acceleration or rate of change of peak pressure, urging a reinterpretation of observations made on time-intensity trading (see, e.g., Irvine et al. 1995).

The target-range sensitivities of neurons in the auditory

system of echolocating bats are also thought to be mediated by coincidence detection (e.g., Sullivan 1986). These neurons are best excited by a particular delay between a component of the pulse emitted by the bat and a component of the returning echo (e.g., O'Neill and Suga 1982). Interestingly, these neurons are tuned to combinations of an echo component with the highest amplitude preceded by the pulse component with the lowest amplitude, and thus likely with the lowest acceleration of peak pressure. This particular selection of pulse and echo components for target range computation is ideal with respect to minimizing the delay requirements of spikes triggered by the pulse so that they coincide at some comparator neuron with the spikes triggered by the echo.

The fact that latency–acceleration/rate of change of peak pressure functions of different neurons are strikingly similar in shape has some interesting consequences for the sequence of first spikes in neuronal populations. Consider a population of neurons that differ in minimum latency and in *S* to a stimulus of a given frequency (Fig. 21, *top, neurons 1–6*). Depending on the acceleration of peak pressure, each of these neurons will fire with a particular delay, and the latency functions of the different neurons can cross each other at different acceleration magnitudes. However, function crossing only occurs for neurons that differ in transient sensitivity and in minimum latency. The latency functions of neurons that share the same sensitivity, but that have different minimum latencies, are only shifted along the ordinate (*neurons 1–3* in Fig. 21, ——). Consequently, the temporal relationships between the first spikes in such a population of neurons are constant and independent of the magnitude of acceleration of peak pressure (Fig. 21, *middle*). Such a temporal pattern could therefore constitute a scale-invariant representation, as recently suggested by Hopfield (1995), of this stimulus parameter. Minimum latencies seem to be laid out in orderly topographic fashions within isofrequency domains of various auditory nuclei (e.g., Heil and Scheich 1991; Heil et al. 1992a; Park and Pollak 1993; Schreiner and Langner 1988). It is therefore conceivable that the detection of such temporal patterns might be mediated through neurons receiving coincident inputs from neurons with some range of minimum latencies. Discharges from the higher-order neurons could then decode the presence of acceleration of peak pressure in a scale-invariant fashion, i.e., such neurons would signal the presence of a transient.

In contrast, the intervals between the first spikes in a population of neurons with similar minimum latencies but different transient sensitivites vary systematically with the magnitude of acceleration (Fig. 21, *bottom*). The temporal dispersion of spikes in such a population increases in an orderly fashion with decreasing acceleration, but the order of succession of first spikes remains unaltered. Thus neurons in such a population would fire at various instances of a transient, and could possibly be used to systematically track instantaneous properties (such as peak pressure, see companion paper) of transients. Because the transient sensitivity of a given neuron is a function of frequency (Fig. 6), this proposed transient tracking would consecutively involve neurons with different CF that are laid out in an orderly tonotopic map. Such a mechanism might contribute to the instantaneous coding of transients thought to underlie the categorical perception of speech and some nonlinguistic sounds (Cutting and Rosner 1974).

Although the present study focuses on the timing of the first spike to isolated tone onsets, similar relationships between latency and acceleration/rate of change of peak pressure might hold for signals other than tone bursts and for more rapid sequences of envelope transients. The phase-locking of spikes to various amplitude-modulated signals, as observed at different levels of the auditory pathway (for references see INTRODUCTION), suggests that each cycle effectively constitutes a new onset. The observation that cortical neurons have acceleration-frequency filters (Fig. 6) suggests that a given neuron will ''view'' a spectrally complex signal through this filter, and that the acceleration of the frequency component to which the neuron is most sensitive will determine its response latency. It is worthwhile reemphasizing that every onset, even that of a ''pure tone,'' is spectrally complex. These considerations also suggest that the perceived isochrony of anisochronous musical and speech sounds (Tuller and Fowler 1980; Vos and Rasch 1981) may have its origin in differences in acceleration of peak pressure, rather than in ''. . . adaptation of the hearing mechanism to a certain relative stimulus level . . .'' (Vos and Rasch 1981, p. 323).

Finally, the companion paper reveals that the first-spike latency of a given neuron has an unexpected consequence for the response of the neuron itself.

I am grateful to Drs. D.R.F. Irvine and R. Rajan for help with the experiments; to J. F. Cassell, M. Farrington, V. N. Park, and R. Williams for technical support; to Drs. M. B. Calford, D.R.F. Irvine, and G. K. Yates and two anonymous reviewers for comments on the manuscript; and to many colleagues for critical discussions.

This study was supported by the National Health and Medical Research Council of Australia.

Received 5 August 1996; accepted in final form 26 December 1996.

REFERENCES

AITKIN, L. M., ANDERSON, D. J., AND BRUGGE, J. F. Tonotopic organization and discharge characteristics of single neurons in nuclei of the lateral lemniscus of the cat. *J. Neurophysiol.* 33: 421–440, 1970.

BRUGGE, J. F., DUBROVSKY, N. A., AITKIN, L. M., AND ANDERSON, D. J. Sensitivity of single neurons in in auditory cortex of cat to binaural tonal stimulation: effects of varying interaural time and intensity. *J. Neuophysiol.* 32: 1005–1024, 1969.

CALFORD, M. B. AND SEMPLE, M. N. Monaural inhibition in cat auditory cortex. *J. Neurophysiol.* 73: 1876–1891, 1995.

CARLILE, S. (Editor). The physical and psychophysical basis of sound localization. In: *Virtual Auditory Space: Generation and Application.* Austin, TX: Landes, 1996, p. 27–78.

CLAREY, J. C., BARONE, P., AND IMIG, T. J. Physiology of thalamus and cortex. In: *The Mammalian Auditory Pathway: Neurophysiology,* edited by A. N. Popper and R. R. Fay. New York: Springer-Verlag, 1992, p. 232–334.

CUTTING, J. E. AND ROSNER, B. S. Categories and boundaries in speech and music. *Percept. Psychophys.* 16: 564–570, 1974.

DURRANT, J. D. AND LOVRINIC, J. H. *Basis of Hearing Science* (2nd ed.). Baltimore, MD: Williams & Wilkins, 1984.

EGGERMONT, J. J. Differential effects of age on click-rate and amplitude-modulation-frequency coding in cat primary auditory cortex. *Hear. Res.* 65: 175–192, 1993.

FRISINA, R. D., SMITH, R. L., AND CHAMBERLAIN, S. C. Differential encoding of rapid changes in sound amplitude by second order auditory neurons. *Exp. Brain Res.* 60: 417–422, 1985.

GOLDBERG, J. M. AND BROWN, P. B. Response of binaural neurons of dog

superior olivary complex to dichotic tonal stimuli: some physiological mechanisms of sound localization. *J. Neurophysiol.* 32: 613–636, 1969.

HALL, J. C. AND FENG, A. S. Influence of envelope rise time on neural responses in the auditory system of anurans. *Hear. Res.* 36: 261–276, 1988.

HEIL, P. A previously unrecognized stimulus parameter determines latency of auditory neurons: acceleration of peak pressure. In: *Brain and Evolution. Proceedings of the 24th Goettingen Neurobiology Conference*, edited by. N. Elsner and H.-U. Schnitzler. Stuttgart, Germany: Thieme, 1996, p. 244.

HEIL, P. Auditory cortical onset responses revisited. II. Response strength. *J. Neurophysiol.* 77: 2642–2660, 1997.

HEIL, P. AND IRVINE, D.R.F. Acceleration of peak pressure, not sound pressure level, determines first-spike latency of auditory cortical neurons (Abstract). *Proc. Aust. Neurosci. Soc.* 7: 115, 1996a.

HEIL, P. AND IRVINE, D.R.F. On determinants of first-spike latency in auditory cortex. *Neuroreport* 7: 3073–3076, 1996b.

HEIL, P., LANGNER, G., AND SCHEICH, H. Processing of frequency-modulated stimuli in the chick auditory cortex analogue: evidence for topographic representations and possible mechanisms of rate and directional sensitivity. *J. Comp. Physiol. A Sens. Neural Behav. Physiol.* 171: 583–600, 1992a.

HEIL, P., RAJAN, R., AND IRVINE, D.R.F. Sensitivity of neurons in cat primary auditory cortex to tones and frequency-modulated stimuli. I. Effects of variation of stimulus parameters. *Hear. Res.* 63: 108–134, 1992b.

HEIL, P. AND SCHEICH, H. Functional organization of the avian auditory cortex analogue. II. Topographic distribution of latency. *Brain Res.* 539: 121–125, 1991.

HEIL, P., SCHULZE, H., AND LANGNER, G. Ontogenetic development of periodicity coding in the inferior colliculus of the mongolian gerbil. *Auditory Neurosci.* 1: 363–383, 1995.

HIND, J. E., GOLDBERG, J. M., GREENWOOD, D. D., AND ROSE, J. E. Some discharge characteristics of single neurons in the inferior colliculus of the cat. II. Timing of the discharges and observations on binaural stimulation. *J. Neurophysiol.* 26: 321–341, 1963.

HOPFIELD, J. J. Pattern recognition computation using action potential timing for stimulus representation. *Nature Lond.* 376: 33–36, 1995.

IRVINE, D.R.F., PARK, V. N., AND MATTINGLEY, J. B. Responses of neurons in the inferior colliculus of the rat to interaural time and intensity differences in transient stimuli: implications for the latency hypothesis. *Hear. Res.* 85: 127–141, 1995.

JEFFRESS, L. A. A place theory of sound localization. *J. Comp. Physiol. Psychol.* 41: 35–39, 1948.

JORIS, P. X., CARNEY, L. H., SMITH, P. H., AND YIN, T.C.T. Enhancement of neural synchronization in the anteroventral cochlear nucleus. I. Responses to tones at the characteristic frequency. *J. Neurophysiol.* 71: 1022–1036, 1994.

JORIS, P. X. AND YIN, T.C.T. Responses to amplitude-modulated tones in the auditory nerve of the cat. *J. Acoust. Soc. Am.* 91: 215–232, 1992.

KITZES, L. M., GIBSON, M. M., ROSE, J. E., AND HIND, J. E. Initial discharge latency and threshold considerations for some neurons in cochlear nucleus complex of the cat. *J. Neurophysiol.* 41: 1165–1182, 1978.

LANGNER, G. AND SCHREINER, C. E. Periodicity coding in the inferior colliculus of the cat. I. Neuronal mechanisms. *J. Neurophysiol.* 60: 1799–1822, 1988.

LANGNER, G., SCHREINER, C. E., AND MERZENICH, M. M. Covariation of response latency and temporal resolution in the inferior colliculus of the cat. *Hear. Res.* 31: 197–202, 1987.

MIDDLEBROOKS, J. C., CLOCK, A. E., XU, L., AND GREEN, D. M. A panoramic code for sound location by cortical neurons. *Science Wash. DC* 264: 842–844, 1994.

O'NEILL, W. E. AND SUGA, N. Encoding of target range and its representation in the auditory cortex of the mustached bat. *J. Neurosci.* 2: 17–31, 1982.

OVERHOLT, E. M., RUBEL, E. W., AND HYSON, R. L. A circuit for coding interaural time differences in the chick brainstem. *J. Neurosci.* 13: 2050–2067, 1992.

PARK, T. J. AND POLLAK, G. D. GABA shapes a topographic organization of response latency in the mustache bat's inferior colliculus. *J. Neurosci.* 13: 5172–5187, 1993.

PFEIFFER, R. R. AND KIM, D. O. Response patterns of single cochlear nerve fibers to click stimuli: descriptions for cat. *J. Acoust. Soc. Am.* 52: 1669–1677, 1972.

PHILLIPS, D. P. Temporal response features of cat auditory cortex neurons contributing to sensitivity to tones delivered in the presence of continuous noise. *Hear. Res.* 19: 253–268, 1985.

PHILLIPS, D. P. Effect of tone-pulse rise time on rate-level functions of cat auditory cortex neurons: excitatory and inhibitory processes shaping responses to tone onset. *J. Neurophysiol.* 59: 1524–1539, 1988.

PHILLIPS, D. P. AND HALL, S. E. Response timing constraints on the cortical representation of sound time structure. *J. Acoust. Soc. Am.* 88: 1403–1411, 1990.

PHILLIPS, D. P., HALL, S. E., AND HOLLETT, J. L. Repetition rate and signal level effects on neuronal responses to brief tone pulses in cat auditory cortex. *J. Acoust. Soc. Am.* 85: 2537–2549, 1989.

PHILLIPS, D. P. AND SARK, S. A. Separate mechanisms control spike numbers and inter-spike intervals in transient responses of cat auditory cortex neurons. *Hear. Res.* 53: 17–27, 1991.

PHILLIPS, D. P., SEMPLE, M. N., AND KITZES, L. M. Factors shaping the tone level sensitivity of single neurons in posterior field of cat auditory cortex. *J. Neurophysiol.* 73: 674–686, 1995.

PICKETT, J. M. *The Sounds of Speech and Communication.* Baltimore, MD: University Park, 1980.

PICKLES, J. O. *An Introduction to the Physiology of Hearing* (2nd ed.). London: Academic 1988.

RAJAN, R., IRVINE, D.R.F., AND CASSELL, J. F. Normative N1 audiogram data for the barbiturate-anesthetized domestic cat. *Hear. Res.* 53: 153–158, 1991.

REES, A. AND MØLLER, A. R. Responses of neurons in the inferior colliculus of the rat to AM and FM tones. *Hear. Res.* 10: 301–330, 1983.

RHODE, W. S. AND GREENBERG, S. Physiology of the cochlear nuclei. In: *The Mammalian Auditory Pathway: Neurophysiology*, edited by A. N. Popper and R. R. Fay. New York: Springer-Verlag, 1992, p. 94–152.

RHODE, W. S. AND GREENBERG, S. Encoding of amplitude modulation in the cochlear nucleus of the cat. *J. Neurophysiol.* 71: 1797–1825, 1994.

ROBLES, L., RHODE, W. S., AND GEISLER, C. D. Transient response of the basilar membrane measured in squirrel monkeys using the Moessbauer effect. *J. Acoust. Soc. Am.* 59: 926–939, 1976.

ROUILLER, E., DE RIBAUPIERRE, Y., TOROS-MOREL, A., AND DE RIBAUPIERRE, F. Neural coding of repetetive clicks in the medial geniculate body of the cat. *Hear. Res.* 11: 235–247, 1981.

RUGGERO, M. A. Cochlear delays and traveling waves: comments on ''Experimental look at cochlear mechanics.'' *Audiology* 33: 131–142, 1994.

RUGGERO, M. A. AND RICH, N. C. Timing of spike initiation in cochlear afferents: dependence on site of innervation. *J. Neurophysiol.* 58: 379–403, 1987.

RUSSELL, I. J. AND SELLICK, P. M. Low-frequency characteristics of intracellularly recorded receptor potentials in guinea-pig hair cells. *J. Physiol. Lond.* 338: 179–206, 1983.

SCHREINER, C. E. AND LANGNER, G. Periodicity coding in the inferior colliclus of the cat. II. Topographical organization. *J. Neurophysiol.* 60: 1823–1840, 1988.

SCHREINER, C. E. AND URBAS, J. V. Representation of amplitude modulation in the auditory cortex of the cat. II. Comparison between cortical fields. *Hear. Res.* 32: 49–64, 1988.

SHANNON, R. V., ZENG, F.-G., KAMATH, V., WYGONSKI, J., AND EKELID, M. Speech recognition with primarily temporal cues. *Science Wash. DC* 270: 303–304, 1995.

STEVENS, K. N. Acoustic correlates of some phonetic categories. *J. Acoust. Soc. Am.* 68: 836–842, 1980.

SULLIVAN, W. E. Processing of acoustic temporal patterns in barn owls and echolocating bats: similar mechanisms for the generation of neural place representations of auditory space. *Brain Behav. Evol.* 28: 109–121, 1986.

TULLER, B. AND FOWLER, C. A. Some articulatory correlates of perceptual isochrony. *Percept. Psychophys.* 27: 277–283, 1980.

VAN HEUVEN, V.J.J.P. AND VAN DEN BROECKE, M.P.R. Auditory discrimination of rise and decay times in tone and noise bursts. *J. Acoust. Soc. Am.* 66: 1308–1315, 1979.

VOS, J. AND RASCH, R. The perceptual onset of musical tones. *Percept. Psychophys.* 29: 323–335, 1981.

YIN, T.C.T. AND CHAN, J.C.K. Interaural time sensitivity in medial superior olive of rat. *J. Neurophysiol.* 64: 465–488, 1990.

ZURITA, P., VILLA, A.E.P., DE RIBAUPIERRE, Y., DE RIBAUPIERRE, F., AND ROUILLER, E. M. Changes in single unit activity in the cat's auditory thalamus and cortex associated to different anesthetic conditions. *Neurosci. Res.* 19: 303–316, 1994.